Measuring Non-Markovianity of Noise in the Central Spin System

by

Jiahui Chen

A thesis
presented to the University of Waterloo
in fulfillment of the
thesis requirement for the degree of
Master of Science
in
Physics (Quantum Information)

Waterloo, Ontario, Canada, 2019

I hereby declare that I am the sole author of this thesis. This is a true copy of the thesis, including any required final revisions, as accepted by my examiners.

I understand that my thesis may be made electronically available to the public.

Abstract

In this thesis, we explore non-Markovian noise in the central spin system due to the coupling between the central spin and the environment. We use a solid state nuclear magnetic resonance system to do the experiment since we have control over both the central spin and environment. In particular, we can manipulate the interaction between the central spin and the environment and the interaction between spins from the environment to study their effects individually. A powder of triphenylphosphine is used in the experiment. A change of local field seen by the central spin caused by interaction between spins in the environment is measured experimentally. A quantitative measure of non-Markovianity of noise on the central spin and a method to estimate non-Markovianity using the randomized benchmarking protocol are introduced.

Acknowledgements

First and foremost I would like to thank my supervisor David Cory for giving me the opportunity to work and study in his group and his patient and insightful guidance. He taught me the attitude of doing research.

I would like to thank Xinhua Peng from USTC who has first introduced me to quantum computing. I would also like to thank my committee members Raffi Budakian, Dmitry Pushin who have helped me with many committee meetings and Adam Wei Tsen who has accepted to participate in my defence.

I would like to express my deep gratitude to Mohamad Niknam, Peter Sprenger and Guanru Feng for their friendship and help. They have always been great mentors and friends to me, I owe a great debt to them. I would like to thank Joel Wallman, Joseph Emerson, and Zhaoyang Tian for helpful discussions. It also has been a privilege to work with all the members from Cory group, with special mention to Sangil Kwon, Pan Zheng, Han Le, Guofei Long, Romain Ruhlmann, Zimeng Wang, Dmitry Akhmetzyanov, Dusan Sarenac, Rahul Deshpande, Maryam Mirkamali, and Ian Hinks.

Last but not least, I would like to thank my parents and my partner Lucy for their support and love. They are my reason for waking up every morning.

Dedication

This thesis is dedicated to my grandparents.

Table of Contents

List of Tables

List of Figures

Chapter 1

Introduction

Ever since Richard Feynman suggested the idea that one can use a quantum system to simulate another, many ways have been explored to build such a machine. Through years, it has been realized that such a machine can not only be used to simulate other quantum systems, but can also be used to solve select problems more efficiently than classic computers. However, building a realistic quantum computer is hard due to various practical obstacles (e.g. robust control of the system and scalability). One barrier is the decoherence of quantum information that causes loss of quantum information and decreases precision of control which is due to the coupling between the system and the environment. This Thesis is concerned with methods to characterize the environment seen by a central spin. In particular the goal is to separate Markovian from non-Markovian behaviors.

1.1   Open Quantum System

Quantum mechanics is based on a few fundamental principles and axioms. The information of a quantum system can be summarized with a vector (ray) from a Hilbert space $\mathcal{H}$, usually represented by a "ket" $|\psi\rangle$ in Dirac's notation which represents the quantum state of the system. Second, evolutions of a state are unitary operators acting on the same Hilbert space. There exists a continuous dual of the state Hilbert space $\mathcal{H}^\dagger$ such that $\forall \phi \in \mathcal{H}^\dagger$, $\phi : \mathcal{H} \to \mathbb{C}$, where $\mathbb{C}$ is the complex field. The dual is a linear space of functionals acting on the Hilbert space, the elements from the dual is denoted with a "bra" $\langle b|$ in Dirac's notation, and the inner product of the Hilbert space is defined as the $\langle \phi|\psi \rangle$ for $|\psi\rangle \in \mathcal{H}$ and $\langle \phi| \in \mathcal{H}^\dagger$. We make the correspondence $\langle a| = |a\rangle^\dagger$, and $\langle a|a \rangle = 1$. Observable physical quantities are represented by Hermitian operators acting on the Hilbert space. A

measurement with respect to the observable A projects the state $|\psi\rangle$ onto an eigenvector $|a\rangle$ of the observable, the value of the measurement is the eigenvalue, the probability of such an outcome is $|\langle\psi|a\rangle|^2$. Such measurements are projection-valued measures (PVMs), they are represented by projection operators $\{P_i\}$ with $\sum_i P_i = \mathbb{1}$ and $P_i P_j = \delta_{ij} P_i$. A subspace of a Hilbert space is a linear subspace that inherits the same inner product from the Hilbert space. A Hilbert space can be formed of the tensor product of Hilbert subspaces. A bipartite system is a composite system consisting of two subsystems. Suppose the Hilbert spaces of two subsystems are $\mathcal{H}_1$ and $\mathcal{H}_2$ respectively, then the Hilbert space of the bipartite system is $\mathcal{H} = \mathcal{H}_1 \otimes \mathcal{H}_2$. The transformations a system can undergo form a group, therefore if the Hilbert space of the system is of dimension n, the transformation group of all possible unitary transformations is $\mathrm{SU}(n)$. The group of transformations on a bipartite system is $\mathrm{SU}(n_1 \times n_2)$, where n_1 and n_2 are the dimensions of the Hilbert subspaces. The reduction of $\mathrm{SU}(n_1) \otimes \mathrm{SU}(n_2)$ follows the Clebsch-Gordan's rule.

A physical statistical mixture is described by a density matrix

$$\rho = \sum_i p_i |a_i\rangle\langle a_i|, \tag{1.1}$$

where $\sum_i p_i = 1$ and $p_i > 0$ for all is. With this definition $\rho^\dagger = \rho$ and $\mathrm{Tr}(\rho) = 1$. Such a state is a proper mixed state. Eq. (1.1) is a pure state decomposition of the ensemble. Such a decomposition is not unique. A mixture can be viewed as a mixture of pure states no matter how the state was prepared. The set of density matrices is a subset of the Liouville space. The purity of a density matrix is defined as $\mathrm{Tr}(\rho^2)$ which is one if and only if the density matrix represents a pure state. For a proper mixed state a unitary operation acts as $U\rho U^\dagger$. The outcome of a PVM is $\mathrm{Tr}(\rho A)$ for some observable A. A density matrix description is also describing only part of an entangled composite system. For a measurement on a subsystem of a bipartite system, the only function that preserves the outcome is the partial trace [1], the stochastic property of the subsystem is included in the reduced state $\rho_s = \mathrm{Tr}_e(\rho)$. In general an operator that takes a density matrix to a density matrix is described by a completely positive and trace preserving (CPTP) operator. The most general form of measurement is a positive-operator valued measure (POVM). In an open quantum system, one only has knowledge about the subsystem under study without fully knowing the environment. In practice, any quantum system in experiment is an open quantum system due to inevitable coupling to the environment. It can be proved that any CPTP map (POVM) on a system can be viewed as a unitary evolution (PVM) on a larger system, this is the Stinespring's [2] (Naimark's [3]) dilation theorem. This duality suggests the special statistical property of an open quantum system could result from its coupling to an unknown external environment (higher degrees of freedom).

An ensemble system behaves similarly as an open quantum system. For example when an inhomogeneous field is applied on an ensemble system, the ensemble undergoes a sum of unitary evolutions which is not unitary. Moreover, both proper and improper mixed states can be purified. These properties show similarities between ensemble systems and open quantum systems.

1.2   Non-Markovian Processes

A CPTP operator is in general not reversible. For example, the relaxation process of an open quantum system increases the entropy of the system and is irreversible. However, processes like relaxation are still deterministic, making it relatively easy to analyze. In general, if the evolution of an open quantum system is both deterministic and smooth, one can find a master equation to describe the time evolution of the system. Such a process is Markovian. There are more general forms of master equations [4, 5, 6, 7], and a Markovian process is defined as a solution that is derived under a memoryless approximation [8, 9].

Non-Markovian processes need not be CPTP maps and indeed some non-Markovian processes can not be represented by maps. This is due to the existence of the implicit variable which represents the memory of the system. The memory can be either stored in an external environment that is coupled to the system or the special paths the system took. Non-Markovian processes can be found in both open quantum systems and ensemble systems. In chapter 4, a mathematical formulation for non-Markovian processes in ensemble systems will be given and used to study the non-Markovian processes in the central spin system.

1.3   Central Spin System

One of the simplest models for studying the system environment interaction is the central spin model where a single spin-1/2 spin is coupled to an external environment [10, 11, 12]. We are interested in correlations between the central spin and the environment. Information exchange and correlations are the reason for non-Markovian noise on the central spin. Such correlation has been studied in quantum dots with linked-cluster expansion methods [13, 14, 15, 16, 17] and recently by Niknam with solid state nuclear magnetic resonance (NMR) [18, 19]. In this thesis, we use solid state NMR [19] to characterize the central spin system. We have control over both the central spin and the environment, and the coupling between them [20, 21, 22, 23].

The central spin system is described by the following Hamiltonian

$$H = H_s + H_e + H_{\mathrm{int}}. \tag{1.2}$$

Here, H_s is the Hamiltonian of the central spin, H_e is the Hamiltonian of the environment, and H_{int} is the Hamiltonian of the interaction between the central spin and the environment. The central spin exchanges information with the environment through the interaction term H_{int}, developing a correlation with the environment. The information shared in the environment can act as a new source of information, leading to a backflow of information to the central spin, resulting in a non-Markovian behavior. Moreover, the dynamics of the environment plays a very important role, it can be regarded as a mixing process that partially destroys the information shared in the environment, so that the noise on the central spin becomes less dependent on the memory of the environment. Such process will result in a decrease of non-Markovianity, a quantity that measures how non-Markovian a process is, of the noise. However, as will be shown in later chapters, the symmetry of the environment plays a critical role in determining the portion of information that can be destroyed. And it is the goal of the thesis to study the origin of non-Markovian behavior in the central spin system, how to quantize it, and how the dynamics in the environment can make a difference.

1.4   Outline of the Thesis

In this thesis, a solid state NMR system is used to study the central spin system. In the second chapter, a few important experimental concepts and techniques are introduced. In the third chapter, we discuss how to detect the change of local field seen by the central spin caused by the mixing process in the environment and present the data obtained. In the fourth chapter, we introduce the mathematical formula for describing non-Markovian processes in ensemble systems, a measure of non-Markovianity, how to generalize the method to the central spin system, and how to use randomized benchmarking to measure non-Markovianity in experiments. In the fifth chapter, a brief conclusion and a summary of potential future work are given.

Chapter 2

NMR of Dipole Coupled Spins

We choose a solid state NMR system to study the central spin problem since the dipolar interactions is time independent and spectrally resolved. A spin is associated with a magnetic moment, therefore its evolution under an external magnetic field is an element from the SU(2) group. Due to the isomorphism between su(2) and so(3), one can adopt a classical or a semi-classical description for the interaction between spins and external fields. The classical one is captured by the Bloch equations

$$\frac{d\vec{M}}{dt} = \gamma \vec{M} \times \vec{B} + \Gamma, \tag{2.1}$$

where γ is the gyromagnetic ratio, $\vec{M}$ is the macroscopic magnetization of the sample bulk, $\vec{B}$ is the external field placed along the $\hat{z}$ direction and

$$\Gamma = \left(-\frac{M_x}{T_2}, -\frac{M_y}{T_2}, -\frac{M_z - M_0}{T_1} \right) \tag{2.2}$$

is the relaxation term, describing the transverse decoherence and longitudinal relaxation. A semiclassical description exploits the Bloch sphere picture for SU(2) group, where the density matrix vector on the sphere corresponds to the "direction" of the spin explicitly. With help of the semiclassical description, one can explain single spin-1/2 dynamics.

2.1 System Hamiltonians

In the experiments, we are only interested in a few terms of the Hamiltonian: Zeeman interaction, chemical shift, dipolar interaction and control Hamiltonians. The Zeeman

term describes the Zeeman splitting of energy levels of a spin in an external field, and it is the dominant part of the Hamiltonian in high field NMR experiments. The initial state of a system is the thermal equilibrium state of the Zeeman Hamiltonian. The interaction frame defined by the time evolution under the Zeeman term is the rotating frame, control or measurement in the experiments are made within the rotating frame.

The dipolar interaction exists amid objects that have magnetic moments. The direct interaction between two spin-1/2 spins through magnetic field is described by the dipolar interaction Hamiltonian.

$$H_D = -\frac{\mu_0 \gamma_1 \gamma_2 \hbar^2}{16\pi r^3}[3(\sigma_1 \cdot \hat{r})(\sigma_2 \cdot \hat{r}) - \sigma_1 \sigma_2], \tag{2.3}$$

where r is the distance between the two spins and $\hat{r}$ is the unit vector connecting the two spins. The secular part of the homonuclear dipolar Hamiltonian is

$$H_{\text{homo}} = -\frac{\mu_0 \gamma^2 \hbar^2}{32\pi r^3}(3\cos^2\theta - 1)\left(2\sigma_z\sigma_z - \sigma_x\sigma_x - \sigma_y\sigma_y\right). \tag{2.4}$$

Here, we have omitted the tensor product notation between Pauli matrices. We will do so in all following discussions. For heteronuclear interaction, the secular dipolar Hamiltonian is

$$H_{\text{hete}} = -\frac{\mu_0 \gamma^2 \hbar^2}{16\pi r^3}(3\cos^2\theta - 1)\sigma_z\sigma_z. \tag{2.5}$$

The sample we use to explore the central spin model is triphenylphosphine prepared in powder form (Fig. 2.1). In our experiment, we use a spherical bulb to contain the sample so that the external magnetic field inside the sample is uniform. As shown in the figure, in one molecule there is one phosphorus spin and fifteen proton spins. We omit the spins of carbon 13 nuclei whose natural abundance is about 1.1%. The Hamiltonian that includes the terms that are important for the experiment is

$$H = H_{\text{chemical shift}} + H_{\text{hete}} + H_{\text{homo}}, \tag{2.6}$$

where

$$H_{\text{chemical shift}} = \delta\sigma_z^{\text{CS}},$$

$$H_{\text{hete}} = \sigma_z^{\text{CS}} \sum_{i=1}^{15} \omega_i \sigma_z^i,$$

$$H_{\text{homo}} = \sum_{1 \leq i < j \leq 15} \omega_{ij}(2\sigma_z^i \sigma_z^j - \sigma_x^i \sigma_x^j - \sigma_y^i \sigma_y^j), \tag{2.7}$$

6
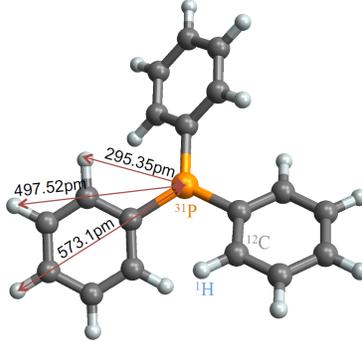
Figure 2.1: Structure of triphenylphosphine molecule reproduced from [18]. There are fifteen proton spins as the environment spins and one phosphuros spin as the central spin. The coupling strength is dependent on the relative orientation of the molecule with respect to the external field. The possible strongest homonuclear interaction between proton spins is 49.8 kHz and the possible strongest heteronuclear interaction is 11.8Hz.

where δ is the chemical shift anisotropy for the central spin, ω_i's and ω_{ij}'s are coupling strengths defined in Eqs. (2.5) and (2.4). The above expressions of the Hamiltonians are for a single molecule, all the coefficients depend on the specific orientation of the molecule with respect to the external static field. In the experiment, we use a sample prepared in a powder form, in which every possible orientation of the molecule in the three dimensional space is equally probable. For the chemical shift, in the principal axis system of the molecule, the chemical shift anisotropy tensor is diagonal

$$R = \begin{pmatrix} \delta_{xx} & & \\ & \delta_{yy} & \\ & & \delta_{zz} \end{pmatrix}. \tag{2.8}$$

Let

$$\begin{aligned} \sigma &= \frac{1}{3}\text{Tr}(R), \\ r &= \delta_{zz} - \sigma, \\ \eta &= \frac{\delta_{yy} - \delta_{xx}}{r}, \end{aligned} \tag{2.9}$$

α, β and γ be the Euler angles describing the position of the principal axis system relative to the lab frame, the secular part of the chemical shift is

$$H_{\text{CS, secular}} = \frac{\omega_0 \sigma_z}{2} \left[\sigma + r \left(\frac{3\cos^2 \beta - 1}{2} + \frac{1}{2} \eta \sin^2 \beta \cos 2\gamma \right) \right], \tag{2.10}$$

where ω_0 is the frequency corresponding to the external magnetic field. For the special case when $\eta = 0$, the distribution the chemical shift anisotropy obeys in a power form is

$$p(\delta) = \frac{1}{\sqrt{3}\omega_0 r} \frac{1}{[1 + (2\delta/\omega r)]^{1/2}}, \qquad -\omega_0 r/2 \leq \delta \leq \omega_0 r. \qquad (2.11)$$

Similarly, one can obtain the probability distribution function for the dipolar interaction between two spins, this distribution gives the lineshape known as the Pake doublet. The probability function for the dipolar interaction in a complex molecule is computationally hard to calculate.

2.2 Average Hamiltonian Theory

In this section we give a brief review of the theory of average Hamiltonian and give some examples of applications of the theory. The use of average Hamiltonian theory to design decoupling sequences can be found in [24]. The preliminary problem of average Hamiltonian theory can be stated as following: Let a quantum system evolve under a time dependent Hamiltonian $H(t)$ for time t, what is the time-independent Hamiltonian F such that the evolution of the system is effectively e^{-iFt}? This was solved in terms of the Magnus expansion

$$F = \sum_{k=0}^{\infty} \bar{H}_k(t), \qquad (2.12)$$

where

$$
\begin{aligned}
\bar{H}_0 &= \frac{1}{t} \int_0^t H(t_1) dt_1, \\
\bar{H}_1 &= -\frac{i}{2t} \frac{1}{2} \int_0^t dt_1 \int_0^{t_1} dt_2 [H(t_1), H(t_2)], \\
\bar{H}_2 &= -\frac{1}{6t} \int_0^t dt_1 \int_0^{t_1} dt_2 \int_0^{t_2} dt_3 \left([H(t_3), [H(t_2), H(t_1)]] + [[H(t_3), H(t_2)], H(t_1)] \right), \\
\cdots.
\end{aligned}
\qquad (2.13)
$$

The above result lays the foundation of average Hamiltonian theory, $\bar{H}_0$ is zeroth order approximation, the rest are the correction terms. Now we prove a useful theorem that predicts the effect of strong averaging.

Theorem 2.2.1. *Let $A, B \in su(n)$, and $\exists T > 0$, s.t. $e^{At} = e^{A(t+T)}$ for $\forall t \in \mathbb{R}$. Define the adjoint operator of A acting on $su(n)$, s.t. for $\forall C \in su(n)$, $ad_A(C) = [A, C]$. Therefore there is an invariant subspace $\mathcal{L}$ of $su(n)$ for ad_A that contains B, then*

(i) $\lim_{n\to\infty} e^{nTA+Bt} = \mathbb{1}$, if $det[D(ad_A)] \neq 0$;

(ii) $\lim_{n\to\infty} e^{nTA+Bt} = \exp\left[\sum_i Tr(BE_i^\dagger)E_i t\right]$, if $det[D(ad_A)] = 0$.

Here, $D(ad_A)$ is the representation of ad_A in $\mathcal{L}$ under some orthonormal basis $\{B_i\}$, E_i are basis vectors from $\{B_i\}$ that satisfies $ad_A(E_i) = 0$.

Proof. $\{B_i\}$ spans an invariant subspace for ad_A, thus for $e^{ad_A t}$ for any $t \in \mathbb{R}$, and $n \in \mathbb{Z}$. Therefore $e^{ad_A t}(B)$ can be expressed as a linear combination of the basis vectors from $\{B_i\}$, and the coefficient of a basis vector B_i can be calculated as $f_i(t) = \mathrm{Tr}\left[B_i^\dagger e^{ad_A t}(B)\right]$. Taking the Fourier transform of $f_i(t)$ yields $\mathcal{F}[f_i](\omega) = \mathrm{Tr}\left[B_i^\dagger \delta(\omega - ad_A)B\right]$. Since $f_i(t)$ must be real, and ad_A has finite number of eigenvectors in $\mathcal{L}$, we have

$$f_j(t) = \sum_{k=-m}^{m} A_k^j e^{-ikt} \tag{2.14}$$

for some positive integer m and $A_k = \pm A_{-k}$. If $\det[D(ad_A)] \neq 0$, then 0 is not an eigenvalue of ad_A in $\mathcal{L}$. Thus, $A_0^i = 0$ for $\forall i$. Therefore let $H = aA + B$, moving into the interaction frame defined by $u = e^{aA}$ yields the Hamiltonian $H_I = u^\dagger B u$. There exists $\tau > 0$ such that $\int_0^\tau f_i(t)dt = 0$ and $f_i(t + \tau) = f_i(t)$ for all i. Therefore when $\tau \to 0$ (i.e. $a \to \infty$) we have

$$\mathcal{T}e^{\int_0^\tau H_I(t')dt'} = e^{\int_0^\tau H_I(t')dt'} + O(\tau^2) \to \mathbb{1}, \tag{2.15}$$

where $\mathcal{T}$ is the time ordering operator, thus

$$\mathcal{T}e^{\int_0^t H_I(t')dt'} = \mathcal{T}e^{\int_{N\tau}^{N\tau+\delta} H_I(t')dt'} \cdots \mathcal{T}e^{\int_0^\tau H_I(t')dt'} \to \mathbb{1}. \tag{2.16}$$

Here, $N\tau + \delta = t$, and we have used the fact that $\delta \to 0$ when $\tau \to 0$. Therefore, by moving back to the ordinary frame and noting that T is a period for e^{At}, we obtain the result $\lim_{n\to\infty} e^{nTA+Bt} = \mathbb{1}$.

When $\det[D(ad_A)] = 0$, note that all the terms except A_0^i in $f_i(t)$ average to zero for all is. Since $\{B_i\}$ is an orthonormal basis , the part that is left is $\exp\left[\sum_i \mathrm{Tr}(BE_i^\dagger)E_i t\right]$. $\square$

A direct corollary of the above theorem is that $\lim_{n\to\infty} e^{-i(2n\pi\sigma_s + \sigma_l t)} = e^{-i\delta_{sl}\sigma_s t}$. This result can be used to obtain the rotating wave approximation and the secular approximation.

All terms in the Magnus expansion should be taken into consideration. However, in many practical cases when t is short enough, $\bar{H}_0$ is more important than other correction terms since it is obvious from magnus expansion that $e^{-i\bar{H}_0 t}$ gives a first order approximation of the evolution. Waugh used average Hamiltonian theory to design the WHH-4 sequence for homonuclear interaction decoupling and demonstrated the power of coherent averaging in spin space [25, 26]. Since then average Hamiltonian theory has been used to explain many sequences and averaging processes in quantum mechanics, dynamical averaging technique has been used to manipulate system Hamiltonians in various quantum systems.
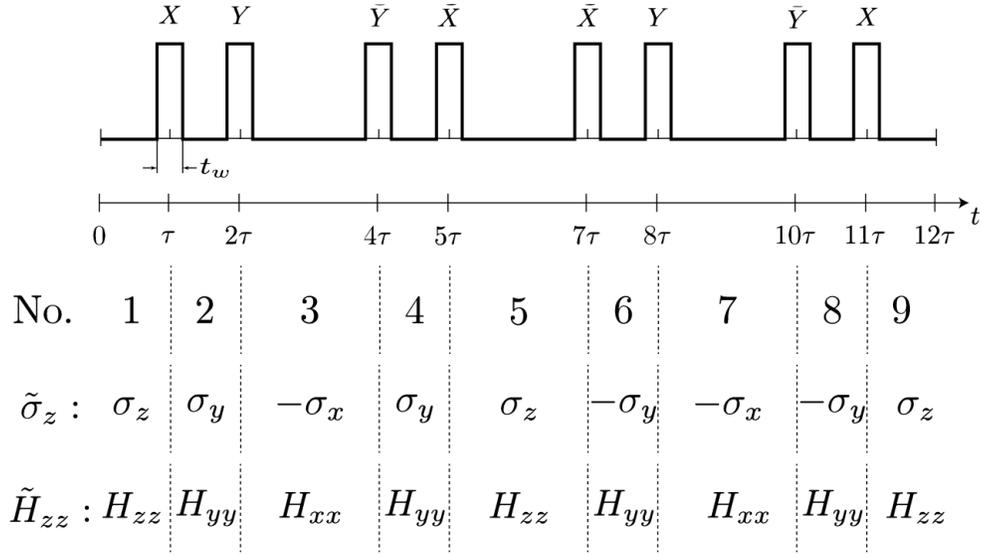
Figure 2.2: Schemiatic for MREV-8 sequence. The MREV-8 sequence is shown at the top, a timeline is shown below it. The effective Hamiltonians of σ_z and H_{zz} in the toggling frame during different windows are shown below.

The sequence used in the experiment for decoupling interactions between proton spins in the environment is the MREV-8 sequence (Fig. 2.4). Here, X, Y, $\bar{X}$ and $\bar{Y}$ represent $\pi/2$ pulses around x, y, $-x$ and $-y$ axes respectively. The sequence was first proposed by Mansfield [27] and by Rhim, Elleman, and Vaughan in 1973 [28] to realize robust decoupling of the homonuclear dipolar interaction. There are decoupling sequences that are more robust than MREV-8 such as BR-24 [29] and Cory-48 [30], but the MREV-8 sequence gives us a good compromise between complexity and resolution. The MREV-8 sequence is composed of two WHH-4 sequences with different phases, and it is cyclic. For a cyclic sequence $U = E_1 P_1 E_2 \cdots P_m E_{m+1}$ where P_i's stand for pulses, E_i's stand for free

evolutions and $E_i = e^{-it_i H}$ for some H one wants to manipulate, and t_i is the length of the ith window, we have $P_1 \cdots P_m = \mathbb{1}$. Therefore, the sequence can be written as

$$U = E_1 P_1 E_2 \cdots P_m E_{m+1} = P_m^\dagger \cdots P_1^\dagger E_1 P_1 \cdots P_m \cdots P_m^\dagger E_m P_m E_{m+1} = \tilde{E}_1 \cdots \tilde{E}_{m+1}, \quad (2.17)$$

where

$$\begin{aligned} \tilde{E}_i &= e^{-it_i \tilde{H}_i}, \\ \tilde{H}_i &= P_m^\dagger \cdots P_i^\dagger E_i P_i \cdots P_m \end{aligned} \quad (2.18)$$

for $i = 1, \cdots, m$, and $\tilde{E}_{m+1} = e^{-it_{m+1} \tilde{H}_{m+1}}$ with $H_{m+1} = H$. Hence, the whole evolution under the sequence can be regarded as one under a piece wise constant Hamiltonian, the frame defined by $P_m^\dagger \cdots P_i$ is called the toggling frame. Therefore, when the total length of the sequence $T = \sum_i t_i$ is small (here we assume the pulses are infinitely strong thus the duration of each pulse is zero), one can use the zeroth order term of the Magnus expansion $\bar{H}_0 = \frac{1}{T} \sum_{i=1}^{m+1} t_i \tilde{H}_i$ to approximate F. If we define the Hamiltonian of the "$\alpha\alpha$" interaction between spin i and spin j as

$$H_{\alpha\alpha}^{ij} = 3\sigma_\alpha^i \sigma_\alpha^j - \sigma^i \cdot \sigma^j \quad (2.19)$$

for $\alpha = x$, y or z, where $\sigma^i \cdot \sigma^j = \sigma_x^i \sigma_x^j + \sigma_y^i \sigma_y^j + \sigma_z^i \sigma_z^j$, it can be seen from Fig. 2.4 that the average Hamiltonian of $H_{\text{homo}} = \sum_{1 \le i < j \le n} \omega_{ij} H_{zz}^{ij}$ is zero for both WHH-4 and MREV-8 sequences. The WHH-4 sequence is also symmetric $H(t) = H(T - t)$, which is a property that the MREV-8 sequence does not have. It can be proved that all the odd order correction terms of the Magnus expansion are zero for a symmetric sequence, in this sense WHH-4 is even better than MREV-8. However in practice, MREV-8 always gives a much narrower line than WHH-4. This is because the MREV-8 sequence accounts for finite pulses and is more robust to B_1 inhomogeneity and common flip angle error [31]. Another important factor that influences the experiment is how σ_z is being averaged under the sequence, this directly affects the form of average Hamitonians of the chemical shift and the heteronuclear interaction. For MREV-8 the direction of the average Hamiltonian of σ_z, namely the axis of effective field, is along $(-1, 0, 1)$ with a scaling factor [18]

$$S = \frac{\sqrt{2} \left[1 + 2\frac{3t_w}{T} \left(\frac{4}{\pi} - 1 \right) \right]}{3}, \quad (2.20)$$

where t_w is the length of each pulse and T is the total length of the MREV-8 sequence. For our experiment the total length of an MREV-8 sequence is $48\mu s$, the length of a proton $\pi/2$ pulse is $2\mu s$, therefore the scaling factor is about 0.504. Because the direction of the effective field is not along z axis, a magnetization precessing around the effective field

11

projects an ellipse on the $x - y$ plane leads to a spectrum of two individual peaks. There are two different components of a magnetization one that is perpendicular to the effective field and another that is along the effective field. The component parallel to the effective field does not feel the B_0 inhomogeneity, and thus decays much slower, resulting in a dc offset in the free induction decay. The signal is a combination of the two different decays. This type of effect always appears in a WHH-4 experiment [32] when a single preparation pulse is used, but does not appear when the initial magnetization is along the y axis in an MREV-8 experiment. In order to obtain a single peak that corresponds to the signal perpendicular to the effective field, a phase cycling is required where a quadrature detection is implemented in the tilted precession plane with respect to the direction of the effective field. This is often accomplished by a combination of two pulses $90°)_x - 45°)_{\text{adjust}}$. Note here that a better performance of MREV-8 is achieved when it is implemented slightly off-resonance (about 1kHz off) due to off-resonance averaging, since a strong effective field partially average out correction terms of the Magnus expansion, leading to a narrower line width.
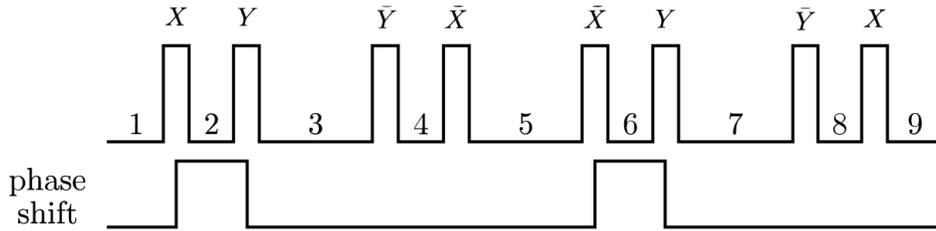
Figure 2.3: Schemiatic for MREV-8 sequence with a phase shift. In the second averaging experiment, the same phase shift is implemented for the first two pulses and the two pulses sandwiching window 6. By introducing the phase shift, an additional field is introduced perpendicular to the direction of the effective field.

Another important technique for improving the performance of the decoupling sequence is using second averaging [33] (Fig. 2.3). The idea is to introduce additional σ_z terms in "some" windows by changing the phases of the pulses by the sides of the window. Second averaging is mostly used to average out unwanted terms along the effective field e.g. chemical shift anisotropy and inhomogeneity of external field, therefore the direction of the additional field should be perpendicular to the direction of the effective field. Sometimes, an additional field that is not perpendicular to the effective field is used to scale down chemical shift, since only the component perpendicular to the direction of the additional field is being averaged. In the example shown in Fig. 2.3, since the direction of the effective field is along $(-1, 0, 1)$, we choose to introduce an additional field along $(1, 0, 1)$. In order

to achieve this, a phase shift ϕ is introduced for the pulses by the sides of the second window and the sixth window. Therefore the sequence becomes

$$
\begin{aligned}
&e^{-i\sigma_z \frac{\phi}{2}} X e^{i\sigma_z \frac{\phi}{2}} e^{-i\sigma_z \frac{\phi}{2}} Y e^{i\sigma_z \frac{\phi}{2}} Y \bar{X} e^{-i\sigma_z \frac{\phi}{2}} \bar{X} e^{i\sigma_z \frac{\phi}{2}} e^{-i\sigma_z \frac{\phi}{2}} Y e^{i\sigma_z \frac{\phi}{2}} \bar{Y} X \\
=&e^{-i\sigma_z \frac{\phi}{2}} X Y e^{i\sigma_z \frac{\phi}{2}} Y \bar{X} e^{-i\sigma_z \frac{\phi}{2}} \bar{X} Y e^{i\sigma_z \frac{\phi}{2}} \bar{Y} X \\
=&e^{-i(\sigma_x + \sigma_z)\phi} + O(\phi^2).
\end{aligned} \tag{2.21}
$$

Note here that the first order approximation $e^{-i(\sigma_x + \sigma_z)\phi}$ is dependent on the phase shift ϕ only so that even a small phase shift corresponds to a strong field. The effective strength can be calculated as $\omega_{\text{eff}} = \frac{2\phi}{\tau}$. Also a small phase shift is recommended regarding the accuracy of the first order approximation in the above equation. Here, we compare experimental data obtained with ordinary MREV-8 sequence and another with second averaging on powder-form adamantane (Fig. 2.4), It can be seen the decay of the sequence with second averaging is much slower, indicating a much better narrowing effect.
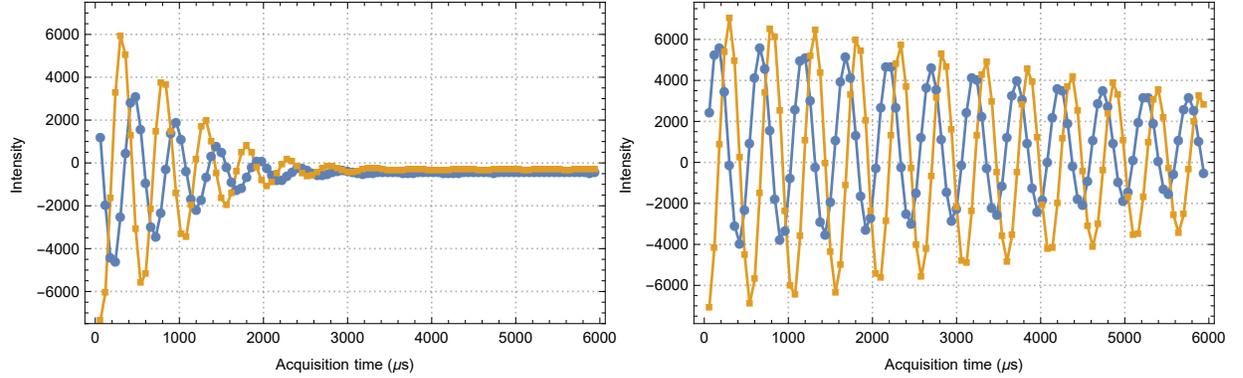
Figure 2.4: Proton signals obtained with MREV-8 sequence on adamantane sample with a single scan. The picture on the left is the time domain data obtained with the ordinary MREV-8 sequence, while the one on the right is obtained with the MREV-8 sequence with second averaging. The length of one MREV-8 sequence is $60\mu s$, one complex point is acquired for each MREV-8 sequence. There are 100 complex data points collected in total for both results, corresponding to a acquisition time of $6000\mu s$. A phase shift of $10°$ is chosen for second averaging for the result on the right. The linewidth corresponding to the left one is 400Hz, while the one corresponding to the right one is 65Hz.

2.3 Tune-up Methods

Successful implementation of decoupling sequences is crucial for our experiment, thus minimizing pulse imperfection that affects performance of the sequence is the first step before implementing the experiment. There are many kinds of pulse imperfection in experiments, the three we focus to minimize are B_1 inhomogeneity, flip angle error that is common to all pulses, and a phase transient error. B_1 inhomogeneity is due to the geometry of the coil and sample, nuclei at different positions feel different strengths of the B_1 field. B_1 inhomogeneity is reduced by changing the geometry of the coil [34].

The flip angle error is due to misadjustment of pulse length and power, it leads to an incomplete decoupling of dipolar interactions and a change of the scaling factor. Phase transient error is due to the reactance of the probe. During the rising and the falling of the pulse, there is an out-of-phase component which is the phase transient error. It can been shown that phase transient is inevitable in a resonance circuit, but symmetric phase transient is harmless for implementation of a decoupling sequence. A detailed discussion of how flip-angle error and phase transient error affect the MREV-8 sequence can be found in [24]. There are other errors such as phase error and individual flip angle error, these errors are small. An experiment such as a phase altering cycle shows these errors are small enough in our experiment. Therefore for the following discussion, we assume the power level is the same for all phases, and there is no phase error or timing error. (Actually in practice, we always tune the probe for all phases to make sure the errors are simultaneous minimized for different phases.)

We mainly follow the tune-up methods described in [35, 36, 37]. Consider the flip-flip cycle (Fig. 2.5 (b)), for perfect pulse if one detects after each pulse, one expects a response like "positive-zero-negative-zero-$\cdots$". If the cycle is repeated n times, one expect four distinguished lines corresponding to different responses. When there is flip angle error, the unitary evolution of the pulse becomes $Xe^{-i\epsilon\sigma_x}$ where ϵ is a small real number. Since the error commutes with the pulses, after a full cycle the remaining term is $e^{-i4\epsilon\sigma_x}$, which gives a sinusoidal modulation of the response. A simple model for phase transient is given by $e^{-i\delta_1\sigma_y}Xe^{-i\delta_2\sigma_y}$ where the $\pi/2$ x rotation is sandwiched by two out-of-phase components with different amplitudes. Since the flip-flip cycle is cyclic, one can apply average Hamiltonian theory to calculate the effect of the phase transient error

$$
\begin{aligned}
&e^{-i\delta_1\sigma_y}Xe^{-i\delta_2\sigma_y}e^{-i\delta_1\sigma_y}Xe^{-i\delta_2\sigma_y}e^{-i\delta_1\sigma_y}Xe^{-i\delta_2\sigma_y}e^{-i\delta_1\sigma_y}Xe^{-i\delta_2\sigma_y}\\
=&e^{-i\delta_1\sigma_y}Xe^{-i(\delta_1+\delta_2)\sigma_y}Xe^{-i(\delta_1+\delta_2)\sigma_y}Xe^{-i(\delta_1+\delta_2)\sigma_y}Xe^{-i\delta_1\sigma_y}\\
=&\mathbb{1}+O(\delta^2),
\end{aligned}
\tag{2.22}
$$

14
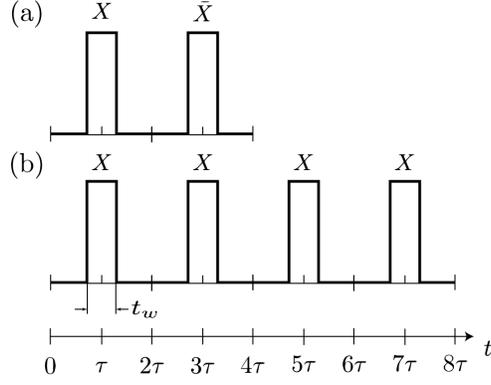
Figure 2.5: Tune-up cycles. (a) is the flip-flop cycle composed of two $\pi/2$ pulses of alternated phases, and (b) is the flip-flip cycle composed of four $\pi/2$ pulses of the same phase. The x phase is shown as an example, but in practice we run the same experiment for all phases.

where δ is a positive real number that bounds δ_1 and δ_2. This means the phase transient error does not affect the response to the flip-flip sequence to the 0th order average Hamiltonian (actually all the odd order correction terms vanish due to the symmetry of the cycle). For the flip-flop cycle (Fig. 2.5 (a)), assume the pulses are perfect, if we detect after each pulse and implement the cycle n times, one expects two lines corresponding to a positive response and a zero response. It is obvious that the flip angle error does not affect the response to the flip-flop cycle since they are canceled out after a full cycle. For the phase transient error, if we detect after $\bar{X}$ pulses, we can calculate the evolution under the average Hamiltonian as

$$
\begin{aligned}
e^{-i\delta_1\sigma_y} X e^{-i\delta_2\sigma_y} e^{i\delta_1\sigma_y} \bar{X} e^{i\delta_2\sigma_y} &= e^{-i\delta_1\sigma_y} X e^{-i(\delta_2-\delta_1)\sigma_y} \bar{X} e^{i\delta_2\sigma_y} \\
&= e^{-i(\delta_2-\delta_1)(\sigma_z-\sigma_y)} + O(\delta^2).
\end{aligned}
\tag{2.23}
$$

With a similar calculation, it can be obtained that the evolution under the average Hamiltonian of the phase transient is $e^{-i(\delta_2-\delta_1)(\sigma_z+\sigma_y)}$ if we detect after X pulses. This means the flip-flop sequence directly measures the difference between the phase transient amplitudes, and when the phase transients are not symmetric, one expects a sinusoidal modulation on each response. Therefore, the strategy for tuning a probe is that we use flip-flip cycle to minimize the flip angle error, and the flip-flop cycle to minimize the phase transient error. If we detect after each pulse in both cycles, when a good tuning is achieved, four distinguished lines corresponding to "positive", "zero", "negative" and "zero" responses for the flip-flip cycle, and two lines corresponding to "positive" and "zero" responses for the flip-

15

flop cycle should be observed. The intensities of the two lines corresponding to "positive" and "negative" responses for the flip-flip cycle should be maximized to achieve minimal flip angle error, and the two lines for the flip-flop cycle should be parallel to each other when the phase transient error is minimized. In our experiment for tuning the probe, the two experiments are implemented on-resonance with a liquid sample, and the two experiments are always done in iteration to achieve a global optimum.
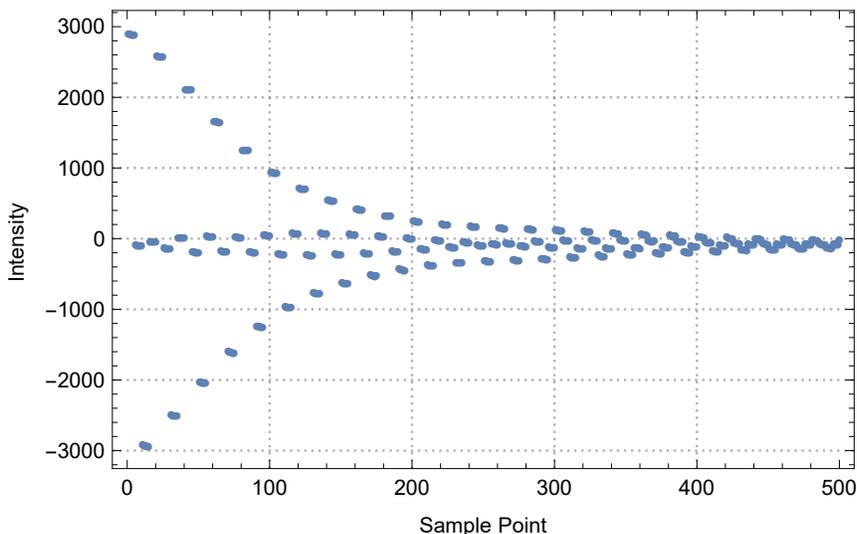
Figure 2.6: Proton signals obtained with flip-flip cycles (only real part). The cycle is repeated 25 times (in total 100 pulses), five data points are sampled after each pulse. It can be seen that the result mainly follows the "positive-zero-negative-zero-···" pattern, indicating a small flip angle error. The five points after the same pulse are approximately on the same level since the experiment is implemented on resonance. The decay of the signal is due to the inhomogeneity of the control field.

A liquid sample that contains rich proton spins (e.g. water) is used to tune up the probe due to its strong signal and long coherence time. The flip angle of a pulse can be adjusted by changing the power or the length of the pulse. In our experiment, we use maximal power (150W) of the spectrometer for implementing MREV-8, thus the flip angle error is minimized by adjusting the length of the pulse only. Fig. 2.6 shows the result of a good tuning for flip angle error. The symmetry and length of phase transient can be adjusted by changing the Q factor of the probe, which is done by changing the matching capacitor of the probe. Usually, the tuning capacitor should be subtly adjusted to obtain an optimal symmetry of the phase transient. A satisfactory phase transient is achieved when there is

16
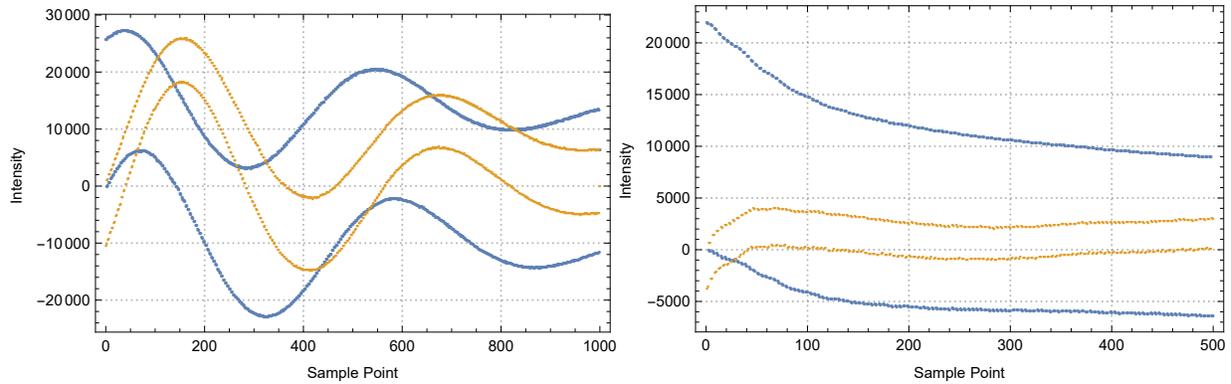
Figure 2.7: Proton signals obtained with flip-flop cycle. The blue dots correspond to the real part of the signal and the orange dots correspond to the imaginary part of the signal. The cycle is repeated 250 times, corresponding to 500 pulses in total. Two data points are sample after each pulse. On the left, a result with asymmetric phase transient is shown, note the two lines corresponding to the real of imaginary part carry a sinusoidal modulation due to the phase transient. On the right, a result with almost symmetric phase transient is shown. It can be seen the two lines corresponding to the real or imaginary part are parallel to each other, indicating a small phase transient error.

about 50% power reflected. And it is very important to have the probe over-coupled to ensure minimal loss of signal to noise ratio. In Fig. 2.7, we compare the results of a good tuning and a bad tuning for phase ransient error using the flip-flop cycle. We note here there are other tune-up methods described in the literature [38].

Chapter 3

Detecting a Change of Local Field

In this chapter, the experiment for measuring a change of local field in the central spin system is discussed. As we mentioned in the introduction, due to memory of the environment, the noise on the central spin system is non-Markovian in general. However one expects a more Markovian noise when a mixing process is introduced in the environment, since the memory is partially destroyed by the mixing process. Therefore in order to better understand the transition between Markovian and non-Markovian noises, it is important to correctly characterize the mixing process. In the central spin system, the central spin communicates with the environment via the heteronuclear interaction

$$H_{\text{hete}} = \sigma_z^{\text{CS}} \sum_i \omega_i \sigma_z^i. \tag{3.1}$$

If the central spin system starts with the initial state $\rho_0 = \sigma_x^{\text{CS}} \mathbb{1}^{\otimes n}$, under the heteronuclear interaction the central spin develops correlations of different orders with the environment. When there is the homonuclear interaction in the environment, due to the flip-flop process

$$\sigma_z \mathbb{1} \xrightarrow{e^{-i\omega(2\sigma_z\sigma_z - \sigma_x\sigma_x - \sigma_y\sigma_y)t}} \frac{1}{2} \left\{ [1 + \cos(4\omega t)] \sigma_z \mathbb{1} + [1 - \cos(4\omega t)] \mathbb{1}\sigma_z + \sin(4\omega t) \left(\sigma_y\sigma_x - \sigma_x\sigma_y \right) \right\}, \tag{3.2}$$

the correlations between the central spin and the environment are mixed, resulting in a destruction of correlations and loss of information. This fact can be rephrased in the picture of local fields in a more general way. Consider a more general form of interaction Hamiltonian between the central spin and the environment

$$H_e = A^{\text{CS}}B, \tag{3.3}$$

where A acts on the space of the central spin, and B is a nondegenerate operator acting on the space of the environment. The evolution of the initial state under H_e can therefore be described as

$$e^{-iH_e t}\left(\sigma_x^{\mathrm{CS}}\mathbb{1}^{\otimes n}\right)e^{iH_e t} = e^{-iA^{\mathrm{CS}}Bt}\left(\sigma_x^{\mathrm{CS}}\sum_{i=1}^{2^n}|i\rangle\langle i|\right)e^{iA^{\mathrm{CS}}Bt}$$

$$= \sum_{i=1}^{2^n} e^{-i\Omega_i tA}\sigma_x^{\mathrm{CS}}e^{i\Omega_i tA}|i\rangle\langle i|, \tag{3.4}$$

where $B|i\rangle = \Omega_i|i\rangle$. Here, Ω_i's are the strengths of the local fields seen by the central spin. Therefore, if $[A^{\mathrm{CS}}, \sigma_x^{\mathrm{CS}}] \neq 0$, the state of the central spin can be regarded as an improper mixture evolving under different local field. Suppose the dynamics of the environment is described by the Hamiltonian H_m, if $[H_m, B] \neq 0$, evolutions under H_m would change the eigenstructure of A, resulting in a mixing of local fields. In our experiment, B corresponds to $\sum_i \omega_i \sigma_z^i$, and H_m corresponds to H_{homo}. This picture is best compared with a spin ensemble evolving under a static field gradient, if one implements an echo experiment, spatial replacement of spins will lead to a change of local fields and an attenuation of the echo [39]. That is the motivation for choosing an experiment similar to the stimulated echo experiment to measure the mixing process in the central spin system. Also since in NMR experiments, we have good control over the system, thus average Hamiltonian theory can be used to manipulate the system Hamiltonian in a desired way, allowing us to study the effect of heteronuclear and homonuclear interactions separately.

3.1 Experimental Design

We want to design an experiment that achieves a unitary evolution as shown in Fig. 3.1 on the central spin system. Assume the initial state of the system is $\rho_0 = \sigma_x^{\mathrm{CS}}\mathbb{1}^{\otimes N}$, if the observable being measured at the end of the experiment is also $\sigma_x^{\mathrm{CS}}\mathbb{1}^{\otimes N}$, a formal expression of the signal of the experiment can be given as

$$S(t_1, t_2) = \frac{1}{d}\langle\sigma_x^{\mathrm{CS}}\mathbb{1}^{\otimes N}|e^{i\hat{H}_{\mathrm{hete}}t_2}e^{-i\hat{H}_{\mathrm{homo}}\Delta}e^{-i\hat{H}_{\mathrm{hete}}t_1}|\sigma_x^{\mathrm{CS}}\mathbb{1}^{\otimes N}\rangle$$

$$= \frac{1}{d}\left(\sum_n\langle\sigma_x|e^{i\Omega_n\hat{\sigma}_z^{\mathrm{CS}}t_2}\langle a_n|\right)e^{-i\hat{H}_{\mathrm{homo}}\Delta}\left(\sum_m|a_m\rangle e^{-i\Omega_m\hat{\sigma}_z^{\mathrm{CS}}t_1}|\sigma_x\rangle\right) \tag{3.5}$$

$$= \frac{1}{d}\sum_{n,m}\langle\sigma_x|e^{i(\Omega_n t_2 - \Omega_m t_1)\hat{\sigma}_z^{\mathrm{CS}}}|\sigma_x\rangle\langle a_n|e^{-i\hat{H}_{\mathrm{homo}}\Delta}|a_m\rangle,$$

19

$$\boxed{\;e^{-iH_{\text{hete}}t_1}\;\Big|\;e^{-iH_{\text{homo}}\Delta}\;\Big|\;e^{iH_{\text{hete}}t_2}\;}$$
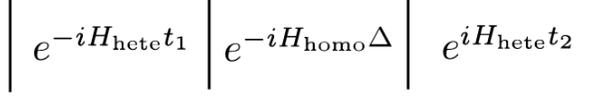
Figure 3.1: Schematic for the experiment measuring the change of local field. In this experiment, we want separate the effect of heteronuclear interaction and homonuclear interaction, so that we can realize an experiment that is like "evolution under local field-mixing-inverse evolution under local field". With this experiment, we can compare the difference of local field before and after the mixing, thus measuring the effect of mixing.

where d is the dimension of the Liouville space, $\hat{B}|a_i\rangle = \Omega_i|a_i\rangle$ where $B = \sum_i \omega_i \sigma_z^i$, and $|\mathbb{1}^{\otimes N}\rangle = \sum_n |a_n\rangle$. The states and the unitary evolutions are all represented in the Liouville space, the hat notation above an operator refers to its conjugation action, and a representation such as $\langle a|\hat{B}|c\rangle$ should be understood as $\text{Tr}(a^\dagger BcB^\dagger)$ in the corresponding Hilbert space. Therefore, when $\Delta = 0$, since $\langle a_n|a_m\rangle = \delta_{nm}$, $S(t_1, t_1) = 1$. When $\Delta \neq 0$, $\langle a_n|e^{-i\hat{H}_{\text{homo}}\Delta}|a_m\rangle$ gives the conditional probability of the change of local field, the intensity is therefore dependent on $e^{-i\hat{H}_{\text{homo}}\Delta}$. For a complex system such as the central spin system in our experiment, due to many configurations of the coupling constant, the local field the central spin sees should be described by a probability distribution function, the effect of $e^{-i\hat{H}_{\text{homo}}\Delta}$ can be characterized by a conditional probability function. If we denote the local field before mixing by Ω, that after mixing by Ω', the distribution function of the local field by $\rho(\Omega)$, and the conditional probability function describing change of local field by $p(\Omega'|\Omega)$, the result of the experiment can be written as

$$S(t_1, t_2) = \int_{-\infty}^{\infty} \int_{-\infty}^{\infty} e^{-i\Omega t_1} \rho(\Omega) p(\Omega'|\Omega) e^{i\Omega' t_2} d\Omega d\Omega'. \tag{3.6}$$

In order to see the process more clearly, we use a functional decomposition of the conditional probability as $p(\Omega'|\Omega) \approx \sum_{k=-l}^{l} p_k(-\Omega + r_k\Omega')$, where $r_k < r_{k+1}$ for all k. According to the convolution theorem

$$\int_{-\infty}^{\infty} \int_{-\infty}^{\infty} g(\omega) f(-\omega + a\omega') d\omega e^{-i\omega't} d\omega' = \frac{1}{a} \tilde{g}(at)\tilde{f}(at) \tag{3.7}$$

for any $f, g \in L^1(\mathbb{R})$, we have

$$S(t_1, t_2) = \sum_{k=-N}^{k=N} \frac{1}{r_k} \tilde{\rho}[r_k(t_2 - t_1)]\tilde{p}_k(r_k t_2), \tag{3.8}$$

20

where the tilde denotes the inverse Fourier transform of the function. As an example, assume $p(\Omega'|\Omega) = p(\Omega' - \Omega)$ and takes the form of a Gaussian function, then $S(t_1, t_2)$ is also modulated by a Gaussian decay. If we further assume that $\tilde{\rho}[r_k(t_2 - t_1)]$ is centered at 0, then we obtain the attenuation is approximately dependent on t_1 in the form of a Gaussian function. For an infinite environment the longer the system evolves under the heteronuclear interaction, the more sensitive it is to the mixing process. This argument is consistent with intuition and the experiment done by Niknam [18]. In general, the function $p(\Omega'|\Omega)$ depends on H_{homo}, and can be very complex.

The experiment we designed to realize the above purpose is shown in Fig. 3.2. The first
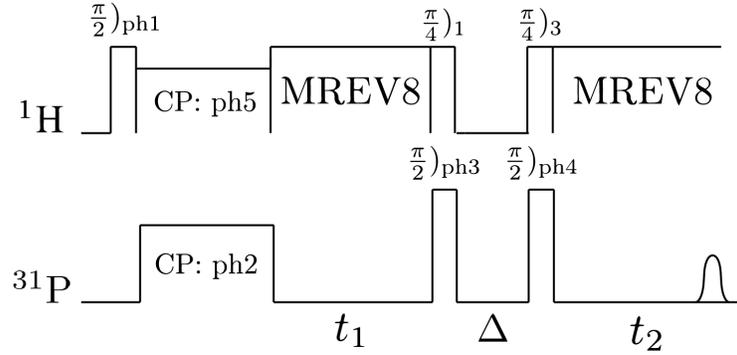
Figure 3.2: Pulse sequence of the experiment for measuring change of local field. The first part of the experiment is cross-polarization for transferring polarization from proton spins to phosphorus spins. The second part is a stimulated-echo-like pulse sequence for realizing the scheme plotted in Fig. 3.1. The phases of each pulse and continuous waves are shown in Table 3.1. The pulses $\frac{\pi}{4})_1$ and $\frac{\pi}{4})_3$ on proton spins after t_1 rotate pronton magnetization from the direction of the effective field of the MREV-8 sequence to z direction and back after mixing.

part of the experiment is cross-polarization denoted by "CP" for preparing the the initial state $\rho_0 = \sigma_x^{\mathrm{CS}} \mathbb{1}^{\otimes n}$, where the the central spin is polarized along x axis and the environment is in the fully mixed state. The rest of the experiment is a stimulated-echo-like experiment for realizing the unitary evolution depicted in Fig. 3.1. The stimulated echo experiment has been a standard experiment to measure the effect of diffusion process [40]. We note here there are other choices for measuring the decoherence caused by the mixing process in the environment [41, 42]. A typical stimulated echo experiment is shown in Fig. 3.3, the 2nd echo that appears after τ after the last pulse is the stimulated echo, τ is the length of the window between the first and second pulses. The magnetization contributing to the stimulated echo is stored along the quantization axis during the storage time (Δ), thus it is

not affected by the local field during that window. This corresponds to the window where we introduce the mixing in our experiment. The experimental design is very similar to that used in measuring spin diffusion [43, 44, 45]. Note in our experiment, the first preparation pulse in stimulated echo experiment is substituted by the cross-polarization process.
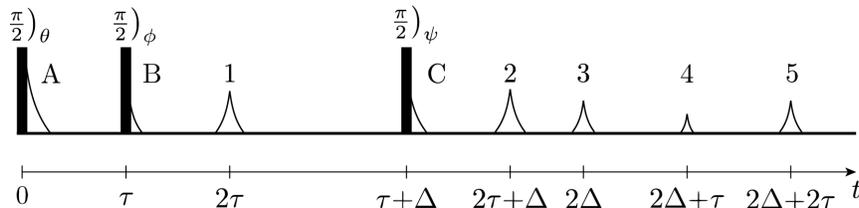
Figure 3.3: Pulse sequence for stimulated echo experiment. The first pulse is to rotate the magnetization of spins from the z axis to the $x - y$ plane. There is one echo at τ after the second pulse and four echoes at τ, $\Delta - \tau$, Δ, and $\Delta + \tau$ after the last pulse respectively. The phase dependence of the echoes on the pulses can be calculated using the k-space formula, and summarized in Table. 3.2. The echo at τ after the last pulse (echo 2) is the stimulated echo.

A phase cycling (Table 3.1) is designed to remove the artifacts and unwanted signals in the experiment. The phases of free induction decays only depend on the pulses right before, while the phases of echoes can be calculated using the k-space formula [46], the result is summarized in Table 3.2. Spin temperature alteration and quadrature detection are also included in the phase cycling to remove the artifact from the cross-polarization and misalignment.

The t_1 and t_2 periods in Fig. 3.2 correspond to the first and last windows in Fig. 3.3 respectively. The MREV-8 sequence is used to decouple the homonuclear interaction during the two windows. Since the direction of effective field under the MREV-8 sequence is $(-1, 0, 1)$, it is important to rotate the magnetization of the proton spins back to the quantization axis during the mixing process, and rotate it back to $(-1, 0, 1)$ after mixing. This is the reason for the two pulses on proton spins sandwiching the mixing window (Fig. 3.2). In the next section, we will present the data collected from the experiment.

3.2 Data and Discussion

We implemented the experiment shown in Fig. 3.2 on a Bruker 300MHz high resolution solid state NMR system. The tune-up cycles are used to minimize the pulse imperfection.

Table 3.1: Phase cycling of experiment in Fig. 3.2. Here, 0, 1, 2, and 3 correspond to 0°, 90°, 180°, and 270° respectively. A full cycle requires at least 16 scans, while we run 32 scans in our experiment.

ph1	ph2	ph3	ph4	ph5	ph31
1	0	0	0	0	0
1	0	0	0	2	2
1	2	2	0	0	0
1	2	2	0	2	2
1	1	1	1	0	1
1	1	1	1	2	3
1	3	3	1	0	1
1	3	3	1	2	3
1	0	1	1	0	2
1	0	1	1	2	0
1	2	3	1	0	2
1	2	3	1	2	0
1	1	2	2	0	3
1	1	2	2	2	1
1	3	0	2	0	3
1	3	0	2	2	1

Table 3.2: Phase dependence of echoes in the stimulated echo experiment calculated using the k-space formula. Note here θ is the phase of the initial state.

No.	Phase
1	$-\theta + 2\phi$
2	$-\theta + \phi + \psi$
3	$\theta - 2\phi + 2\psi$
4	$\frac{\pi}{2} - \phi + 2\psi$
5	$-\theta + 2\psi$

The length of a $\pi/2$ pulse on proton spins is $1.65\mu s$, that on phosphorus spins is $1.4\mu s$. The length of each MREV-8 cycle is $48\mu s$, therefore, t_1 and t_2 are incremented in step of $48\mu s$. The experiment is repeated for different t_1's and Δ's, and the data is acquired continuously during t_2. t_1 is chosen from $48\mu s, 96\mu s, \cdots, 384\mu s$, Δ is chosen from the set

$$\{10\mu s, 15\mu s, 20\mu s, 30\mu s, 50\mu s, 70\mu s, 90\mu s, 110\mu s, 130\mu s, 150\mu s, 170\mu s, 190\mu s, 210\mu s,$$
$$230\mu s, 250\mu s, 300\mu s, 400\mu s, 600\mu s, 800\mu s, 1000\mu s, 1500\mu s, 2000\mu s, 2500\mu s\}$$
$$(3.9)$$

and for each combination of t_1 and Δ, twenty complex points are sampled during t_2 with the delay between each two adjacent points being $48\mu s$. A few echoes from the experiment are shown in Fig. 3.4.

Afterwards, a Fourier transform is taken for each echo. The integral of the magnitude of the Fourier transforms are plotted in Fig. 3.5.
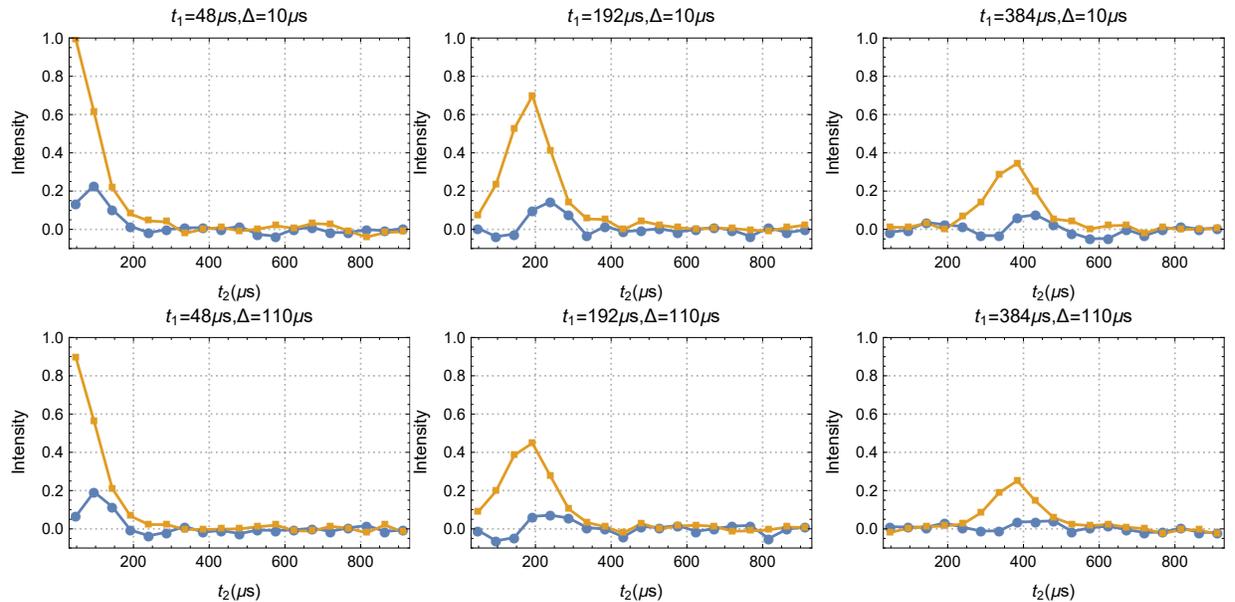
Figure 3.4: Stimulated echoes measured on phosphorus spins. The blue points correspond to the real part of the signal, while orange points correspond to imaginary part of the signal. The y axis is the intensity of the signal normalized with respect to the first point of the first echo (the amplitude of the first complex point in the figure on the top left corner). It can be seen from the plot, the amplitude of the echoes decays as t_1 increases (from the left to the right). The decay with respect to Δ is not so prominent.
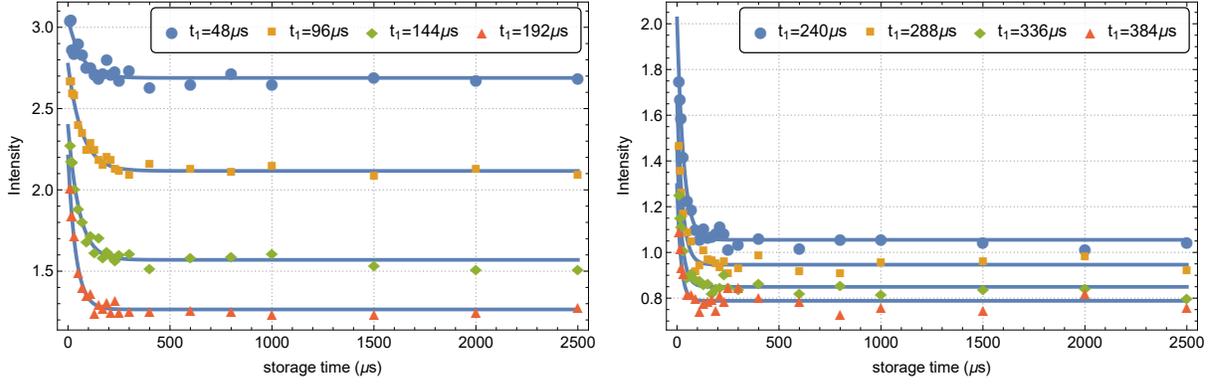
Figure 3.5: Plot of amplitudes of echoes with respect to Δ for different t_1s. The blue lines are plots of exponential fitting of the data points. The decay is faster for larger t_1. The saturation level of the fit is also lower for larger t_1.
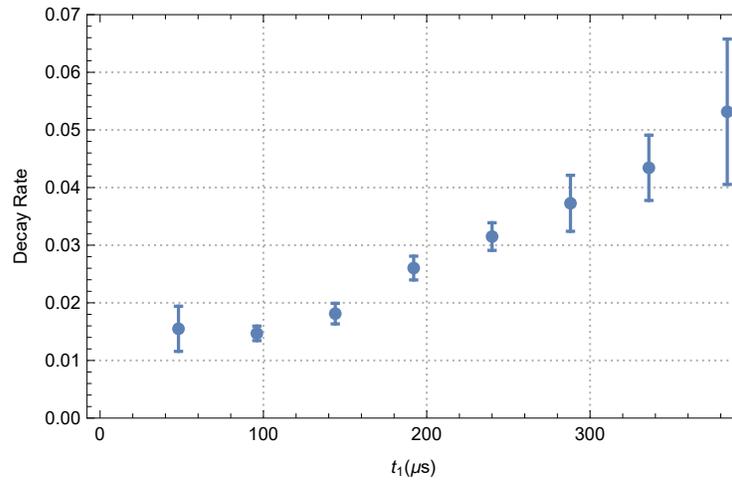
Figure 3.6: Decay rate of the exponential fit for different t_1. The error bars are calculated according to the standard error of the estimate.

In order to measure the decay rate of the intensities of echoes with respect to the storage time Δ, the data is fitted to an exponential function $A + Be^{-r\Delta}$ (blue solid lines in Fig. 3.5). The decay rates are shown in Fig. 3.6.

The intensity of the echo decays as a function of Δ. We choose an exponential function to fit the data for simplicity. The decay rate increases monotonically as a function of t_1, which is consistent with the experimental result obtained by Niknam [18]. This is because with more shared information between the central spin and the environment, the system is more sensitive to perturbation in the environment. Note that in Fig. 3.5, the decays saturate at some point. This is due to the symmetry of the mixing process in the environment. The mixing process is complex. As one possible explanation, suppose all possible mixing processes on the environment of a single molecule form a group G which is a subgroup of $\mathrm{SU}(2^n)$. Since the mixing process may have different effect on different molecules of the ensemble, assume the initial state of the environment is ρ_e, after a mixing process the state of the environment becomes

$$\rho'_e = \int_{g \in G} g\rho_e^g g^\dagger d\tau_g \tag{3.10}$$

for some invariant measure τ_g on G and $\int_{g \in G} \rho_e^g d\tau_g = \rho_e$. When the system is saturated, we have $s\rho'_e s^\dagger = \rho'_e$ for $\forall s \in G$. Therefore, ρ'_e must commute with G, anything else is killed in the process. Hermitian operators that commute with G are defined as symmetries of G. For example, $\sum_i \sigma_z^i$ and $\sigma_z^1 \cdots \sigma_z^n$ are both symmetries of the mixing process in our experiment. Due to the many symmetries of the mixing process, the information is not entirely destroyed. Instead, it is preserved as a symmetry and later gives a non-zero echo. If $G = \mathrm{SU}(2^n)$, the only symmetry is the identity, then any correlation between the central spin and the environment could be destroyed given a mixing process that is long enough. However, we note that $G = \mathrm{SU}(2^n)$ is not a necessary condition for the signal to decay to zero. Actually, as long as the elements that commute with G do not end up as observables, the echo could decay to zero. The fact that the signal monotonically decays until it saturates suggests that it is very similar to a diffusion process. This fact is the fundamental approximation we will take in the next chapter.

Chapter 4

Quantitative Measure of Non-Markovianity

A stochastic chain is a collection of random variables $X(t) = X_t$ on a common probability space [47], where $t \in \mathbb{N}$. Usually X_t takes values from a fixed set $\mathcal{S}$, the state space of the process. The probability of finding the system to be in some specific state s_{n+1} at time $t = n + 1$ given all the previous states of the system is a conditional probability. The process is a Markov chain when the probability only depends on the state of the system at time $t = n$ for all $n \in \mathbb{N}$

$$P(X_{n+1} = s_{n+1} | X_n = s_n, \cdots, X_0 = s_0) = P(X_{n+1} = s_{n+1} | X_n = s_n). \qquad (4.1)$$

Now suppose that the state space is finite, $\mathcal{S} = \{1, 2, \cdots, d\}$, the transition matrix from $t = n$ to $t = n + 1$ of the Markov chain is

$$(M_{n+1,n})_{ij} = P(X_{n+1} = i | X_n = j). \qquad (4.2)$$

When $M_{n+1,n}$ is independent of n the Markov chain is stationary, but in general $M_{n+1,n}$ can be different for different n's. Define the distribution vector in the d-dimensional probability space as

$$\pi_n = (P(X_n = 1), \cdots, P(X_n = d))^T, \qquad (4.3)$$

we have

$$\pi_n = M_{n,n-1} \cdots M_{1,0} \pi_0 \qquad (4.4)$$

where $M_{n,0} = M_{n,n-1} \cdots M_{1,0}$ is a matrix, π_0 is the initial distribution of the system. When the state space is finite, a stochastic chain is Markovian if and only if the the time

evolution of the distribution vector from arbitrary time t_1 to arbitrary time t_2 can be represented as a matrix acting on the probability space. Generalizing the classic definition to quantum mechanics, the distribution vector corresponds to the density matrix of the quantum system and the probability space corresponds to the Liouville space. A quantum process is Markovian if and only if the evolution of the system from arbitrary time t_1 to arbitrary time t_2 can be represented as a matrix acting on the Liouville space. This is equivalent to saying that the evolution from t_1 to t_2 is always linear. Therefore, a measurement of linearity of the evolution gives an estimation of non-Markovianity of the process.

We are interested in two kinds of non-Markovian processes. The first kind is due to the memory stored in the environment, and the second kind is due to different paths taken by different parts of the ensemble system. The state of an ensemble is represented by a density matrix ρ, assume the quantum systems in the ensemble are all closed, they can only undergo unitary evolutions, therefore the evolution the ensemble undergoes can be represented as

$$\rho \longrightarrow \sum_i^N w_i U_i \rho_i U_i^\dagger, \tag{4.5}$$

where $\rho = \frac{1}{N}\sum_i \rho_i$, ρ_i's are density matrices, and $w_i > 0$ is the probability to find a particle of the ensemble to be in the state ρ_i. Here, the decomposition of the density matrix represents the memory of the system, it can be represented by a vector

$$\beta = (w_1\rho_1, \cdots, w_i\rho_i, \cdots, w_N\rho_N). \tag{4.6}$$

In this chapter, we refer to the vector β as the memory of the system, it is a vector in the space $\mathcal{L}^{\oplus N}$, which we refer to as the memory space for simplicity. Each ρ_i is a vector in the Liouville space $\mathcal{L}$. Without ambiguity, the same symbol is used for the density operator and its vector representation in the Liouville space. When $\rho_i = \rho$ for all i, the system is uncorrelated, and the evolution can be reduced to a linear operator. In general the process is not a linear operator on the Liouville space when the system is correlated. The process is linear, therefore Markovian, if and only if $U_i = U$ for all i's. Therefore, it is natural to define the non-Markovianity of the process as a measure of how different the U_i's are on average. Since a good definition of the non-Markovianity of the process should be independent of its arguments, the non-Markovianity should be a function of U_i's and w_i's only. For some metric $d : SU(n) \times SU(n) \to [0, +\infty)$, a measure of nonlinearity of the evolution with respect to the metric d is

$$\xi_d = \sum_{i,j} w_i w_j d(U_i, U_j). \tag{4.7}$$

When the decomposition of the density matrix is dependent on some parameter x (x could be either a number or a vector), the evolution of the density matrix of an ensemble is represented as

$$\rho \longrightarrow \int w(x)U(x)\rho(x)U(x)^{\dagger}dx. \tag{4.8}$$

Then the nonlinearity of the evolution is

$$\xi_d = \iint w(x)w(y)d(U(x), U(y))dxdy, \tag{4.9}$$

and the memory $\beta = w(x)\rho(x)$. ξ_d gives a measure of the non-Markovianity of the process. In the following analysis we will refer to ξ_d as the non-Markovianity for simplicity. Additionally, when d is induced by some norm $\| \cdot \|$, it is translationally invariant and homogeneous

$$\begin{aligned} d(A + C, B + C) &= d(A, B), \\ d(\alpha A, \alpha B) &= |\alpha|d(A, B), \end{aligned} \tag{4.10}$$

and obeys the strong version of the triangle inequality

$$d(A + B, C + D) \leq d(A, C) + d(B, D). \tag{4.11}$$

In this chapter, we are only concerned with d that is induced by a norm. In general, the non-Markovianity of a process is different from the non-Markovianity of a combination of the process with another Markovian process. Sometimes it is convenient to require the non-Markovianity of a process to be independent of the coordinate, namely $d(VU_i, VU_j) = d(U_iW, U_jW) = d(U_i, U_j)$ for arbitrary unitaries V and W. The non-Markovianity defined with such a metric is unitarily invariant. For an open quantum system, however, it is hard to have a similar definition. But as will be seen later, the case of the central spin system can be reduced to a case similar to an ensemble system, thus one can still use Eq. (4.7) to calculate the non-Markovianity. In this chapter, we show how to measure the non-Markovianity in the central spin system using the randomized benchmarking protocol.

4.1 Twirl

Let $M_n(\mathbb{C})$ denote the space of all $n \times n$ matrices with complex entries. For $E \in M_n(\mathbb{C})$, its unitary twirl is defined as

$$E_{\text{twirl}} = \int_{U \in \text{SU}(n)} UEU^{\dagger}d\tau_U. \tag{4.12}$$

Here, $d\tau_U$ is the invariant measure such that $d\tau_U = d\tau_{VU}$ for $\forall V \in \mathrm{SU}(n)$. Therefore,

$$VEV^\dagger = \int_{U \in \mathrm{SU}(n)} VUEU^\dagger V^\dagger d\tau_U = \int_{U \in \mathrm{SU}(n)} UEU^\dagger d\tau_{V^\dagger U} = E. \qquad (4.13)$$

This means $[E_{\mathrm{twirl}}, \mathrm{SU}(n)] = 0$. The twirl is closely related to the average gate fidelity of the operator E [48]

$$\tilde{F}(E) = \int \langle\phi|E|\phi\rangle d\phi = \int_{U \in \mathrm{SU}(n)} \langle\phi|UEU^\dagger|\phi\rangle d\tau_U = \langle\phi|E_{\mathrm{twirl}}|\phi\rangle. \qquad (4.14)$$

Note here the definition of average gate fidelity is the fidelity between E and $\mathbb{1}$. The twirl of an operator preserves the minimal information of the operator about how close the operator is to the identity. There are only two invariant subspaces for the conjugation action of $\mathrm{SU}(n)$ on $\mathcal{L}$: $\{\mathbb{1}\}$ and $\mathcal{L} - \{\mathbb{1}\}$ [49]. Therefore, according to Schur's Lemma, E_{twirl} must be a multiple of the identity in each irreducible subspace. If the identity is chosen as the first basis vector of $\mathcal{L}$, then $E_{\mathrm{twirl}} = \mathrm{Diag}(1, \lambda, \cdots, \lambda)$ where $(n^2 - 1)\lambda + 1 = \mathrm{Tr}(E)$. Here, we have assumed E preserves the identity. Repeated application of E_{twirl} onto some state $\rho \in \mathcal{L}$ yields

$$E_{\mathrm{twirl}}^k(\rho) = \lambda^k \rho + \mathbb{1}(1 - \lambda^k). \qquad (4.15)$$

Therefore, the survival probability of the quantum state is an exponential function of k

$$\mathrm{Tr}\left[\rho E_{\mathrm{twirl}}^k(\rho)\right] = \lambda^k, \qquad (4.16)$$

and

$$\tilde{F}(E) = \lambda + \frac{1 - \lambda}{n}. \qquad (4.17)$$

Benchmarking protocols are based on using the twirl to estimate the average gate fidelity of quantum channels [48]. An efficient benchmarking protocol requires the use of the unitary-t design [50]. Let G be a finite subgroup of $\mathrm{SU}(n)$, G is a unitary-t design if

$$\int_{U \in \mathrm{SU}(n)} P_t(U) d\tau_U = \frac{1}{|G|} \sum_{U \in G} P_t(U), \qquad (4.18)$$

where $P_t(U)$ is a polynomial of U and $U^\dagger$ of order of at most t. Therefore, a unitary-2 design can efficiently achieve twirling. Clifford group is a unitary-2 design. Therefore, the twirl of an operator E can be realized as

$$E_{\mathrm{twirl}} = \int_{U \in \mathrm{SU}(n)} UEU^\dagger d\tau_U = \frac{1}{|\mathcal{C}|} \sum_{i=1}^{|\mathcal{C}|} C_i E C_i^\dagger. \qquad (4.19)$$

Hence, according to the rearrangement theorem

$$E_{\text{twirl}}^k = \frac{1}{|\mathcal{C}|^k} \left(\sum_{i=1}^{|\mathcal{C}|} C_i E C_i^\dagger \right)^k = \sum_{i_1,\cdots,i_k} C_{i_1} E C_{i_2} E \cdots C_{i_{k+1}} = \mathbb{E}_{\vec{C} \in \mathcal{C}^k} \left(C_{i_1} E C_{i_2} E \cdots C_{i_{k+1}} \right),$$

(4.20)

where $C_{i_{k+1}} = (C_{i_1} C_{i_2} \cdots C_{i_k})^\dagger$ and $\vec{C} = (C_{i_1}, \cdots, C_{i_k})$. In the randomized benchmarking protocol, one can estimate $\mathbb{E}_{\vec{C} \in \mathcal{C}^k} \left(C_{i_1} E C_{i_2} E \cdots C_{i_{k+1}} \right)$ by the mean of picking uniformly at random from the Clifford group for m times for each C_{i_j} [51, 52]. Randomized benchmarking protocol is free of state preparation and measurement error. It is a more efficient and reliable way for estimating the average gate fidelity of a unitary-2 design compared to state tomography [53].

Markovian noise on an open quantum system gives rise to an exponential decay in a randomized benchmarking experiment. Any deviation of the decay function from a single exponential function is an indication of the non-Markovianity.

4.2 Measuring Non-Markovianity in the Central Spin System

The fact that the randomized benchmarking protocol is reliable and easy to implement and that Markovian noise results in an exponential decay provides motivation to explore its use to measure the non-Markovianity. In the central spin system, the noise on the central spin is due to the coupling between the central spin and the environment. Therefore, the noise is a function of the evolution under the heteronuclear interaction. This process in general is non-Markvovian, and we want to use a twirl on the central spin to study this non-Markovianity. Especially, we want to study the effect that mixing in the environment has on the non-Markovianity of the noise on the central spin. We implement a randomized benchmarking experiment as described in Fig. 4.1. The experimental design is quite similar to that of symmetrized characterization of noise [54, 55]. Here, since the Clifford gates only act on the central spin. Define

$$\begin{aligned} E &= e^{-iH_{\text{hete}}\tau_e}, \\ M &= e^{-iH_{\text{homo}}\tau_m}. \end{aligned}$$

(4.21)

This protocol implements $\left(\tilde{\Lambda} M \right)^m$, where $\tilde{\Lambda}$ is the partial twirling of the heteronuclear
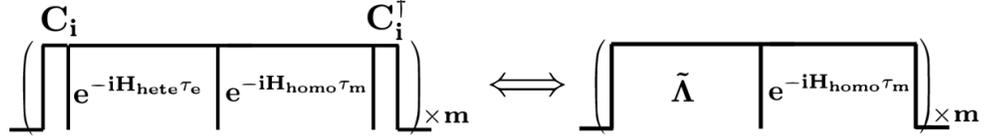
Figure 4.1: Schematic of randomized benchmarking experiment for measuring the non-Markovianity in central spin system. C_i's are Clifford gates acting on the central spin only. The sequence is repeated m times in each experiment with C_i's uniformly at random chosen from the Clifford set of one qubit. Each experiment is repeated many time (300 times in the simulation), and the average of the results of the experiments are taken to obtain the survival probability after m steps. Since the Clifford gates only act on the central spin, one is effectively twirling the evolution under the heteronuclear interaction.

evolution

$$\tilde{\Lambda} = \sum_i C_i \mathbb{1}_e \circ e^{-i\sigma_z \otimes A\tau_e} \circ C_i^\dagger \mathbb{1}_e = \mathbb{1} \otimes \cos(\tau_e A) + (\sigma_z)_{\text{twirl}} \otimes \sin(\tau_e A), \tag{4.22}$$

where $A = \sum_{i=1}^n \omega_i \sigma_z^i$. If the initial state of the system is $\rho_0 = \sigma_x^{\text{CS}} \mathbb{1}$, a simple picture is obtained from the standard local field picture in Eq. (3.4) and note here that $H_e = H_{\text{hete}}$, we have

$$\rho_t^{\text{CS}} = \text{Tr}_e(E\rho_0 E^\dagger) = \text{Tr}_e \left(\frac{1}{2^n} \sum_{i=1}^{2^n} e^{-i\hat{\sigma}_z \Omega_i \tau_e} (\sigma_x) |i\rangle\langle i| \right) = \frac{1}{2^n} \sum_{i=1}^{2^n} e^{-i\hat{\sigma}_z \Omega_i \tau_e} (\sigma_x), \tag{4.23}$$

where $A|i\rangle = \Omega_i$. Therefore, when there is only heteronuclear interaction, the central spin system can be decomposed into 2^n components that evolve under different local fields. This is similar to an ensemble system composed of 2^n single quantum systems, using the definition in Eq. (4.7), the non-Markovianity of the process is

$$\xi_d = \frac{1}{2^{2n}} \sum_{i,j} d \left(e^{-i\hat{\sigma}_z \Omega_i \tau_e}, e^{-i\hat{\sigma}_z \Omega_j \tau_e} \right). \tag{4.24}$$

And the survival probability after m applications of $\tilde{\Lambda}$ is

$$S_m = \frac{1}{2^n} \langle \sigma_x | \sum_{i=1}^{2^n} \left(e^{-i\hat{\sigma}_z \Omega_i \tau_e} \right)_{\text{twirl}}^m |\sigma_x\rangle = \frac{1}{2^n} \sum_{i=1}^{2^n} p_i^m, \tag{4.25}$$

where

$$p_i = \frac{\text{Tr}\left[\left(e^{-i\hat{\sigma}_z \Omega_i \tau_e} \right)_{\text{twirl}} \right] - 1}{d^2 - 1} = \frac{2\cos(2\Omega_i \tau_e) + 1}{3}. \tag{4.26}$$

32

According to [52], the difference of average fidelity of two channels is

$$\Delta \tilde{F}(A, B) = |\tilde{F}(A) - \tilde{F}(B)|, \tag{4.27}$$

then

$$\Delta \tilde{F}(A, B) \leq \parallel A - B \parallel_{1 \to 1}^{H} \leq \parallel A - B \parallel_{\diamond}, \tag{4.28}$$

where $\parallel \cdot \parallel_{1 \to 1}^{H}$ is the one norm restricted to Hermitian input, and $\parallel \cdot \parallel_{\diamond}$ is the diamond norm. For the following quantity

$$\tilde{\xi} = \frac{1}{2^{2n}} \sum_{i,j} |p_i - p_j|, \tag{4.29}$$

the following relation holds

$$0 \leq \tilde{\xi} \leq \xi_{1 \to 1}^{H} \leq \xi_{\diamond}. \tag{4.30}$$

Since both $\xi_{1 \to 1}^{H}$ and $\xi_{\diamond}$ give a measure of the non-Markovianity, measuring $\tilde{\xi}$ always gives a lower bound of the non-Markovianity. In the following discussion, we will refer to $\tilde{\xi}$ as the average non-Markovianity. In general $\Delta \tilde{F}(A, B)$ is not a metric. However, It will be shown later when τ_e is small, p_i is a monotonic function of τ_e and Ω_i, thus we expect larger $\tilde{\xi}$ for longer τ_e. It is not generally possible to obtain an analytic solution if we treat the mixing as an unitary acting on the environment. However, if the mixing is modeled as diffusive, then there is a simple understanding of how it leads to decrease of the non-Markovianity. The well-known models of spin diffusion are an example of such analysis [56, 57, 58].

It is helpful to represent the process as a linear operator acting on the memory space $P : \mathcal{L}^{\oplus N} \mapsto \mathcal{L}^{\oplus N}$

$$P = \begin{pmatrix} \hat{U}_1 & & & \\ & \hat{U}_2 & & \\ & & \ddots & \\ & & & \hat{U}_N \end{pmatrix}, \tag{4.31}$$

where $\mathcal{L}$ is the Liouville space. Therefore,

$$P\beta = \left(\hat{U}_1(\rho_1), \cdots, \hat{U}_N(\rho_N) \right). \tag{4.32}$$

P is a unitary operator. The Liouville space is homomorphic to the memory space, and the homomorphism is represented by the matrix

$$T = (\mathbb{1}, \mathbb{1}, \cdots, \mathbb{1}). \tag{4.33}$$

When there is diffusion, different components of the memory β may mix after a short time δt

$$\beta = \begin{pmatrix} \rho_1 \\ \vdots \\ \rho_{2^n} \end{pmatrix} \rightarrow \begin{pmatrix} \rho_1 \\ \vdots \\ \rho_{2^n} \end{pmatrix} + \begin{pmatrix} d_{11}\rho_1 + \cdots + d_{1,2^n}\rho_{2^n} \\ \vdots \\ d_{2^n,1}\rho_1 + \cdots + d_{2^n,2^n}\rho_{2^n} \end{pmatrix} \delta t, \qquad (4.34)$$

the differential equation for β under a diffusion process is

$$\frac{d\beta}{dt} = D\beta, \qquad (4.35)$$

where $D = (d_{ij})$ and $t \geq 0$. Here, each matrix entry in D should be understood as a multiple of the identity when applied on β. This equation describes a diffusion (exchange) process between finite sites. Because there are no new particles generated in a diffusion process, it is required that $d_{ii} \leq 0$ for all i. And by conservation of number of particles, $\sum_{j=1}^{2^n} d_{ij} = 0$ for all i. When $d_{ii} = 0$, the ith site is a sink since particles can only go into the ith site but never out. A signature of such diffusion process is that, it reaches some equilibrium when $t \to \infty$, the equilibrium only depends on $\sum_i \rho_i$, and the diffusion process monotonically takes the vector towards equilibrium. For an isotropic diffusion, $d_{ij} = d$ for all $i \neq j$, namely

$$D = \begin{pmatrix} -N+1 & 1 & \cdots & 1 \\ 1 & -N+1 & \cdots & 1 \\ \vdots & \vdots & \ddots & \vdots \\ 1 & 1 & \cdots & -N+1 \end{pmatrix} \gamma, \qquad (4.36)$$

where $\gamma > 0$. The equilibrium is $\beta_{\mathrm{eq}} = (\bar{\rho}, \cdots, \bar{\rho})$, where $\bar{\rho} = \frac{1}{2^n}\sum_{i=1}^{2^n} \rho_i$. A system with a memory of β_{eq} is uncorrelated. When the system is uncorrelated, the process can always be written as a linear map acting on the Liouville space. That means if we combine some process P with a diffusion process M as $P = PM$, the non-Markovianity of the new process should be less than that of the old one, since the new process always first erases some meomory. And the non-Markovianity of the process MP should be the same with that of P, since erasing memory after P does not change the state in the Liouville space. Therefore, we give the following generalized form of the non-Markovianity of P

Definition 4.2.1. Let

$$P = \begin{pmatrix} w_{11}\hat{C}_{11} & \cdots & w_{1N}\hat{C}_{1N} \\ \vdots & \ddots & \vdots \\ w_{N1}\hat{C}_{N1} & \cdots & w_{NN}\hat{C}_{NN} \end{pmatrix} \qquad (4.37)$$

act on the memory space $\mathcal{L}^{\oplus N}$, where $w_{ij} > 0$, $\sum_{i,j} w_{ij} = N$ and $\hat{C}_{ij}$s are quantum channels. Any operator of this form is defined as a process on the memory space. The non-Markovianity and the average non-Markovianity of the process are defined as

$$
\begin{aligned}
\xi_d(P) &= \sum_{i,j} w_i w_j d\left(\bar{C}_i, \bar{C}_j\right), \\
\tilde{\xi}(P) &= \sum_{i,j} w_i w_j |p_i - p_j|,
\end{aligned}
\tag{4.38}
$$

where $w_i = \sum_{j=1}^N w_{ji}$, $\bar{C}_i = \frac{1}{w_i} \sum_{j=1}^N w_{ji} \hat{C}_{ji}$, p_i is the decay rate of the depolarizing channel $(\bar{C}_i)_{\text{twirl}}$ and d is a metric on $M_n(\mathbb{R})$.

The non-Markovianity inherits the same unitary invariance from the metric d and obeys the inequality Eq.(4.30), and it is positive definite. Then we have the following theorem.

Theorem 4.2.2. *(Monotonicity of the non-Markovianity) Let P be a process without exchange of particles between different sites acting on the memory space $\mathcal{L}^{\oplus N}$, $M = e^{Dt}$ be an isotropitc diffusion process. Then $\xi_d(MP) = \xi_d(P)$ for any t and $\xi_d(PM) \leq \xi_d(P)$ if $t \geq 0$.*

Proof. Since M has the structure of a semigroup, it is sufficient to prove the theorem in the infinitesimal case. The first part of the theorem is trivial since applying M on P from the left only mixes the components of column vectors of P thus it does not change the sum of the components. When D is isotropic and P is a process without exchange of particles between different sites, $\sum_i w_{ij} = w$ for all j. When D is isotropic, $d_{ij} = (-N\delta_{ij} + 1)d$, then for infinitesimal dt let $M = e^{Ddt} = \mathbb{1} + Ddt$ we have

$$
(PM)_{ij} = (1 - Nddt)w_{ij}\hat{C}_{ij} + \sum_k w_{ik}\hat{C}_{ik}ddt = w'_{ij}\hat{C}'_{ij},
\tag{4.39}
$$

where $w'_{ij} = (1-Nddt)w_{ij} + \sum_k w_{ik}ddt$ and $(PM)_{ij}/w'_{ij}$. Therefore, the average of elements of each column of PM is

$$
\sum_i w'_{ij}\hat{C}'_{ij} = (1 - Nddt)w\bar{C}_j + \sum_k w\bar{C}_k ddt = w'\bar{C}'_j,
\tag{4.40}
$$

where $w' = w$ and $\bar{C}'_j = \sum_i w'_{ij}\hat{C}'_{ij}/w'$. Therefore, the non-Markovianity of the process

35

PM is

$$\xi_d(PM) = \sum_{i,j} w_i' w_j' d(\bar{C}_i', \bar{C}_j')$$

$$= \sum_{i,j} \left\{ w \left[(1 - Nddt)w\bar{C}_i + \sum_k w\bar{C}_k ddt \right], w \left[(1 - Nddt)w\bar{C}_j + \sum_k w\bar{C}_k ddt \right] \right\}$$

$$= \sum_{i,j} w^2 (1 - Nddt) d \left(\bar{C}_i, \bar{C}_j \right)$$

$$\leq \sum_{i,j} w^2 d \left(\bar{C}_i, \bar{C}_j \right) = \xi_d(P).$$

$$(4.41)$$

Note here we have used the homogeneity and translational invariance of d. □

Another important fact is that for D isotropic and any process P,

$$\xi_d \left(\lim_{t \to \infty} P e^{Dt} \right) = 0. \tag{4.42}$$

This is due to the fact that the only equilibrium state of e^{Dt} is $\beta_{\text{eq}} = (\bar{\rho}, \cdots, \bar{\rho})$, thus after long enough the sums of components of columns of PM all become the same, corresponding to a zero non-Markovianity.

If we regard the mixing process in the central spin system as a diffusion process, we have $M = e^{D\tau_m}$. However, M cannot be an isotropic diffusion due to its special symmetry. Indeed, recall that if the mixing is applied to the state $\sum_{i=1}^{2^n} \rho_i |i\rangle\langle i|$, it does not change the number of spin-up spins in $|i\rangle$, therefore, the $|i\rangle$'s corresponding to the same number of spin-up spins span an invariant subspace for mixing. Therefore, if we represent D in the memory space, it must be block-diagonalized

$$D = \begin{pmatrix} D_0 & & & \\ & D_1 & & \\ & & \ddots & \\ & & & D_n \end{pmatrix}, \tag{4.43}$$

and $\dim(D_i) = C_n^i$. For simplicity, assume each D_i is isotropic in the corresponding subspace, thus the equilibrium state in the memory space is

$$\beta_{\text{eq}}' = (\bar{\rho}^{(0)}, \cdots, \bar{\rho}^{(0)}, \cdots, \bar{\rho}^{(n)}, \cdots, \bar{\rho}^{(n)}). \tag{4.44}$$

Here, $\bar{\rho}^{(k)} = \frac{1}{C_n^k} \sum_{s=k} \rho_i$ where ρ_i is the state of the central spin corresponding to the state $|i\rangle\langle i|$ of the environment and s is the number of spin-up spins in $|i\rangle$. We have rearranged the order of the states in β'_{eq} so that states that correspond to the same number of spin-up spins are in the same block, under the same basis we can represent P as

$$P = \begin{pmatrix} \hat{U}_1^{(0)} & & & & & & \\ & \ddots & & & & & \\ & & \hat{U}_1^{(i)} & & & & \\ & & & \ddots & & & \\ & & & & \hat{U}_{C_n^i}^{(i)} & & \\ & & & & & \ddots & \\ & & & & & & \hat{U}_1^{(n)} \end{pmatrix} = \begin{pmatrix} P_0 & & \\ & \ddots & \\ & & P_n \end{pmatrix}, \qquad (4.45)$$

where $\hat{U}_j^{(i)}$ is the ith unitary acting on the jth invariant subspace of mixing and

$$P_i = \begin{pmatrix} U_1^{(i)} & & \\ & \ddots & \\ & & U_{C_n^i}^{(i)} \end{pmatrix}. \qquad (4.46)$$

For any $P = (w_{ij}\hat{C}_{ij})$ acting on the memory space $\mathcal{L}^{\oplus N}$, it is defined as a subprocess if it satisfies all properties of a process except $\sum_{i,j} w_{ij} = 1$. Define a memory subspace of $\mathcal{L}^{\oplus N}$ a linear subspace that is isomorphic to $\mathcal{L}^{\oplus N'}$ for some positive integer N'. Now for convenience, define the following quantity between subprocesses P_1 and P_2 acting on two disjoint memory subspaces $\mathcal{M}_1$ and $\mathcal{M}_2$ of $\mathcal{L}^{\oplus N}$ as

$$\xi_d(P_1, P_2) = \sum_{i,j} w_i^{(1)} w_j^{(2)} d(\bar{C}_i^{(1)}, \bar{C}_j^{(2)}), \qquad (4.47)$$

where $P_\alpha = (w_{ij}^{(\alpha)}\hat{C}_{ij}^{(\alpha)})$, $w_j^{(\alpha)} = \sum_i w_{ij}^{(\alpha)}$ and $\bar{C}_j^{(\alpha)} = \sum_i w_{ij}^{(\alpha)}\hat{C}_{ij}^{(\alpha)}/w_j^{(\alpha)}$ for $\alpha = 1, 2$, then we have the following theorem

Theorem 4.2.3. *Let P_1 and P_2 be subprocesses acting on two disjoint memory subspaces $\mathcal{M}_1 = \mathcal{L}^{\oplus N_1}$ and $\mathcal{M}_2 = \mathcal{L}^{\oplus N_2}$ of $\mathcal{L}^{\oplus N}$, then for an isotropic diffusion process M acting on $\mathcal{M}_1$, the following relations hold*

$$\begin{aligned} \xi_d(MP_1, P_2) &= \xi_d(P_1, P_2), \\ \xi_d(P_1 M, P_2) &\leq \xi_d(P_1, P_2). \end{aligned} \qquad (4.48)$$

Proof. The first half of the theorem is trivial, since applying M on P_1 from the left does not change $\bar{C}_i^{(1)}$. For the second half, since $D = (d_{ij})$ is isotropic, $d_{ij} = (-N_1\delta_{ij} + 1)d$ and $w_j^{(1)} = \sum_i w_{ij}^{(1)} = w^{(1)}$ for all j. Therefore, for infinitesimal dt there is

$$
\begin{aligned}
\xi_d(P_1 M, P_2) &= w^{(1)} \sum_j w_j^{(2)} \sum_i d\left[(1 - Nddt)\bar{C}_i^{(1)} + \sum_k \bar{C}_k^{(1)} ddt, \bar{C}_j^{(2)}\right] \\
&\leq w^{(1)} \sum_j w_j^{(2)} \sum_i \left[(1 - Nddt)d\left(\bar{C}_i^{(1)}, \bar{C}_j^{(2)}\right) + ddt \sum_k d\left(\bar{C}_k^{(1)}, \bar{C}_j^{(2)}\right)\right] \\
&= \sum_{i,j} w^{(1)} w_j^{(2)} d\left(\bar{C}_i^{(1)}, \bar{C}_j^{(2)}\right) = \xi_d(P_1, P_2).
\end{aligned}
$$

$$(4.49)$$

Note here we have used the homogeneity of d and the triangle inequality due to the fact d is always induced by some norm. $\qquad\square$

Using the results of **Theorem V.2.** and **Theorem V.3.** yields the result that $\xi_d(Ee^{Dt}) \leq \xi_d(Ee^{Dt'})$, if $t' \geq t$, where we have used E instead of P to refer to the representation of E in the memory space. Now we draw the following conclusion: when there are only heteronuclear interactions, the process is non-Markovian, and the non-Markovianity of the process is larger for longer τ_e when τ_e is small. When there is mixing, the non-Markovianity of the process decreases as τ_m increases, and the saturation of the non-Markovianity is determined by the symmetry of the mixing. Although the original experiment design depicted in Fig. 4.1 suggests implementing ME instead of EM, the non-Markovianity of ME is equal to that of E. But since the initial state commutes with M, we are effectively implementing EM repeatedly. In the randomized benchmarking experiment, the effect of M accumulates so that for a different m, the randomized benchmarking is measuring a different process, and for a larger m the non-Markovianity of the process is smaller. Therefore, it is important to make sure the survival probability is measured for the same m's when one wants to compare the non-Markovianity of E and EM. The effect of Λ on the memory is omitted. In many practical situations, the diffusion happens at the same time with the evolution, in that case the evolution of the system in the memory space can be describe by the differential equation

$$
\frac{d\beta}{dt} = (-iH + D)\beta, \tag{4.50}
$$

where $-iH$ generates the evolution process and D generates the diffusion. A similar conclusion on the non-Markovianity can be drawn using the perturbation theory.

Now we prove that for small errors in the central spin system, the average non-Markovianity $\tilde{\xi}$ gives an faithful estimation of the non-Markovianity. To this end, we just need to prove that $|p_i - p_j|$ is a metric. Note that the matrix representation of $e^{-i\hat{\sigma}_z \Omega_k \tau_e}$ under the basis $\{\mathbb{1}, \sigma_x, \sigma_y, \sigma_z\}$ is

$$
e^{-i\hat{\sigma}_z \Omega_k \tau_e} = \begin{pmatrix} 1 & & & \\ & \cos 2\Omega_i \tau_e & \sin 2\Omega_i \tau_e & \\ & -\sin 2\Omega_i \tau_e & \cos 2\Omega_i \tau_e & \\ & & & 1 \end{pmatrix},
\tag{4.51}
$$

therefore, when $0 \leq 2\Omega_i \tau_e \leq \pi$, $\mathrm{Tr}(e^{-i\hat{\sigma}_z \Omega_k \tau_e}) = \mathrm{Tr}(e^{-i\hat{\sigma}_z \Omega_l \tau_e})$ if and only if $e^{-i\hat{\sigma}_z \Omega_k \tau_e} = e^{-i\hat{\sigma}_z \Omega_l \tau_e}$. The triangle inequality is trivial

$$
|\cos 2\Omega_i \tau_e - \cos 2\Omega_j \tau_e| \leq |\cos 2\Omega_i \tau_e - \cos 2\Omega_k \tau_e| + |\cos 2\Omega_k \tau_e - \cos 2\Omega_j \tau_e|.
\tag{4.52}
$$

If we choose τ_e such that $2\Omega_i \tau_e \leq \pi$ for all i, according to the above analysis $|p_i - p_j|$ is a metric, thus the average non-Markovianity is a non-Markovianity.

In general $\tilde{\xi}$ is not a faithful measure of the non-Markovianity. For example, for the following process

$$
\rho_t = \frac{1}{2} \left(U_1 \rho_1 U_1^\dagger + U_2 \rho_2 U_2^\dagger \right),
\tag{4.53}
$$

let $U_1 = V U_2 V^\dagger$ for some unitary V. Then

$$
p_1 = \frac{\mathrm{Tr}(\hat{U}_1) - 1}{d^2 - 1} = p_2.
\tag{4.54}
$$

The average non-Markovianity of the process is zero, but it is a non-Markovian process and gives a non-vanishing non-Markovianity. However as proved, the average non-Markovianity always provides a lower bound of the non-Markovianity at worst.

4.3   Simulation

In this section we show simulation results of the randomized benchmarking experiment of a finite ensemble system to test the theory. We choose five proton spins from one phenyl group to simulate the environment. To simulate an ensemble average, we pick 100 different orientations of the external field uniformly at random and calculate the interaction Hamiltonian with respect to each orientation. Then the result of the simulation of a randomized

benchmarking experiment is obtained with the Hamiltonian of each orientation, and the mean value of the 100 results with respect to different orientations is taken as the final result. The twirl is estimated by picking 300 random Clifford sequences and taking the average and the survival probability is measured for $m = 1, 2, 4, 8, 16, 32, 64$.

When there is no mixing, an analytic result can be obtained for a randomized benchmarking experiment. Suppose the local field seen by the central spin obeys a normal distribution function

$$\Omega \sim f(\Omega|0, \sigma^2) = \frac{1}{\sqrt{2\pi\sigma^2}} e^{-\frac{\Omega^2}{2\sigma^2}}. \tag{4.55}$$

In absence of mixing, the signal can be regarded as an average of signals from spins that see different local fields. Therefore the survival probability of the mth step is

$$S(m) = \int [p(\Omega)]^m f(\Omega|0, \sigma^2) d\Omega. \tag{4.56}$$

Using the formula that $\int \exp(ax - bx^2) dx = \exp(\frac{a^2}{4b})\sqrt{\pi}/\sqrt{b}$ for $\mathrm{Re}(b) > 0$, one can obtain

$$\int \cos(2\Omega x)^n e^{-\frac{\Omega^2}{2\sigma^2}} dx = \frac{\sqrt{2\pi\sigma^2}}{2^n} \sum_{k=0}^{n} C_n^k e^{-2\sigma^2 t^2 (2k-n)^2}. \tag{4.57}$$

Therefore,

$$\begin{aligned} S(m) &= \int [p(\Omega)]^m f(\Omega|0, \sigma^2) d\Omega \\ &= \int \left[\frac{2\cos(2\Omega t) + 1}{3} \right]^m \frac{1}{\sqrt{2\pi\sigma^2}} e^{-\frac{\Omega^2}{2\sigma^2}} d\Omega \\ &= \frac{1}{3^m} \sum_{n=0}^{m} C_m^n \sum_{k=0}^{n} C_n^k e^{-2\sigma^2 t^2 (2k-n)^2}. \end{aligned} \tag{4.58}$$

Since the linewidth at half height of the normal distribution is $2\sqrt{2\ln 2}\sigma \approx 2.355\sigma$, one can use the the linewidth of the spectrum of the central spin to determine the value of σ. The analytic result is compare to the simulation result in Fig. 4.2, where σ is obtained from the linewidth of the local field distribution plot of the 100 orientations usedin the simulation (Fig. 4.3).

We choose the average non-Markovianity as the non-Markovianity we want to estimate. The average non-Markovianity is related to the deviation of the decay function from a single exponential function (Fig. 4.4). Some examples of the survival probability obtained in the
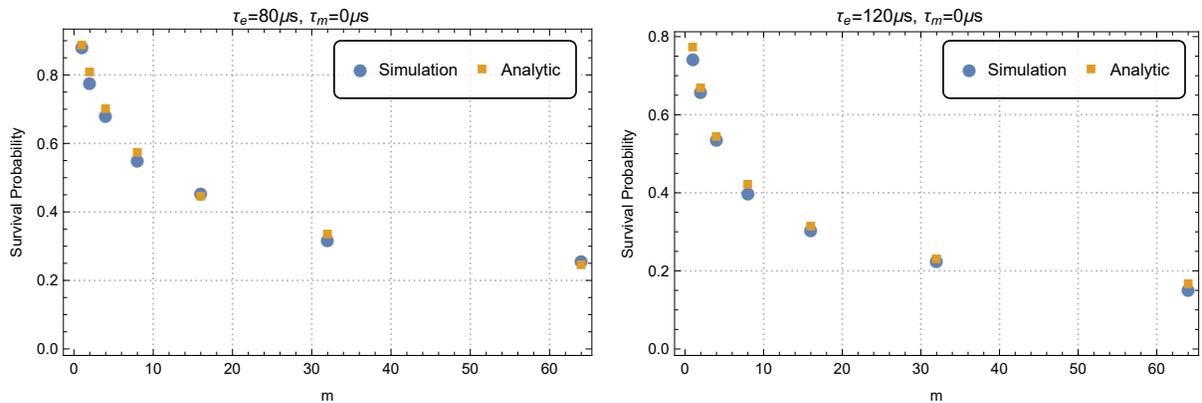
Figure 4.2: Comparison between the theoretical calculation and simulation of randomized benchmarking experiment when there is no mixing. The blue dots correspond to the simulation result and the orange squares correspond to the theoretical calculation. It can be seen they almost coincide.
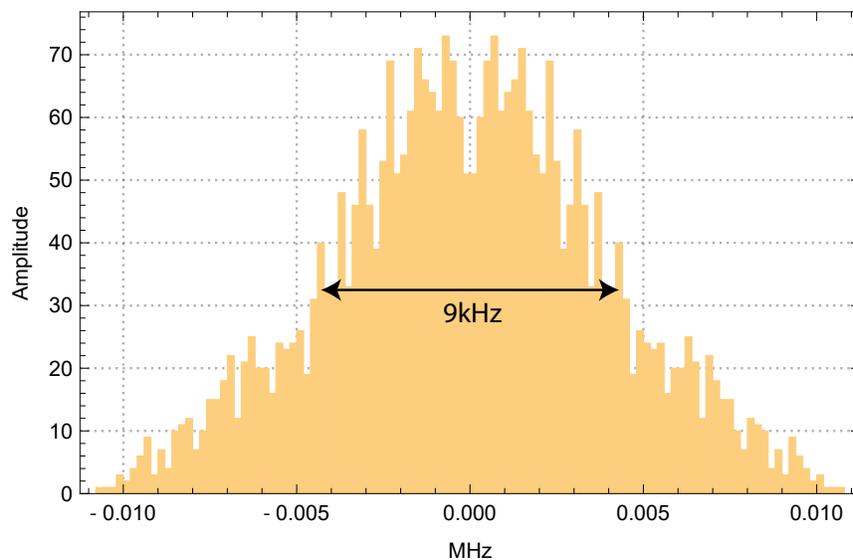
Figure 4.3: Histogram plot of local field of heteronuclear interaction Hamiltonian of 100 different orientations used in the simulation. It can be seen the local field is symmetric about the center, and the approximate half-height width of the distribution is 9kHz.

Figure 4.4: Correspondence between the non-Markovianity and the deviation from single exponential decay. According to the analysis in last section, we expect less non-Markovianity for shorter τ_e and longer τ_m. Since for small error in the central spin system, the average non-Markovianity gives a faithful measure of the non-Markovianity, one can use deviation from a single exponential decay to measure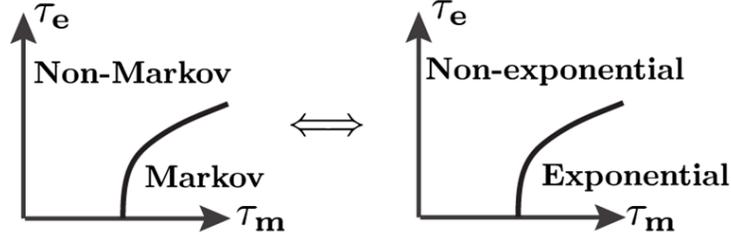 the non-Markovianity. The plot on the left show when τ_e is small and τ_m is large, the process should be more Markovian, corresponding to the plot on the right a less deviation from a single exponential function.

simulation are shown in Fig 4.6, it can be seen that with longer τ_m, the data points are more close to an exponential decay. We use the coefficient of determination (R^2) to measure the deviation. Finding a explicit analytic relation between $\tilde{\xi}$ and R^2 is hard. In Fig. 4.5, N p_i's are generated uniformly at random from the interval $[a, 1]$ and then the survival probability $S(m) = \sum_{i=1}^{N} p_i^m$ as a function of p_i's are calculated for $m = 1, 2, 4, 8, 16, 32, 64$. Then $1 - R^2$ of a single exponential fit to $S(m)$ is calculated, and compared to $\tilde{\xi}$ calculated as a function of p_i's. From the plot we see that when N is large and $\tilde{\xi}$ is small, R^2 gives a good estimate of $\tilde{\xi}$.

In Fig. 4.7, the result of R^2 calculated with respect to survival probability of simulation of different configurations is shown. The result is consistent with the theoretical prediction: For the same τ_e, the greater τ_m is the greater R^2 is; for the same τ_m, the greater τ_e is the less R^2 is before it saturates. The saturation, as we explained, is due to the symmetry of the mixing process. Another interesting phenomenon is that for greater τ_e, R^2 is more sensitive to increase of τ_m. This is also consistent with the argument we made in the last chapter that with more correlation (greater τ_e) between the central spin and the environment, the system is more sensitive to perturbation in the environment (τ_m). The fluctuation is due to statistical error of the simulation and the scale of the environment used in the simulation. However, due to a larger environment, a smoother behavior is expected in the experiment.
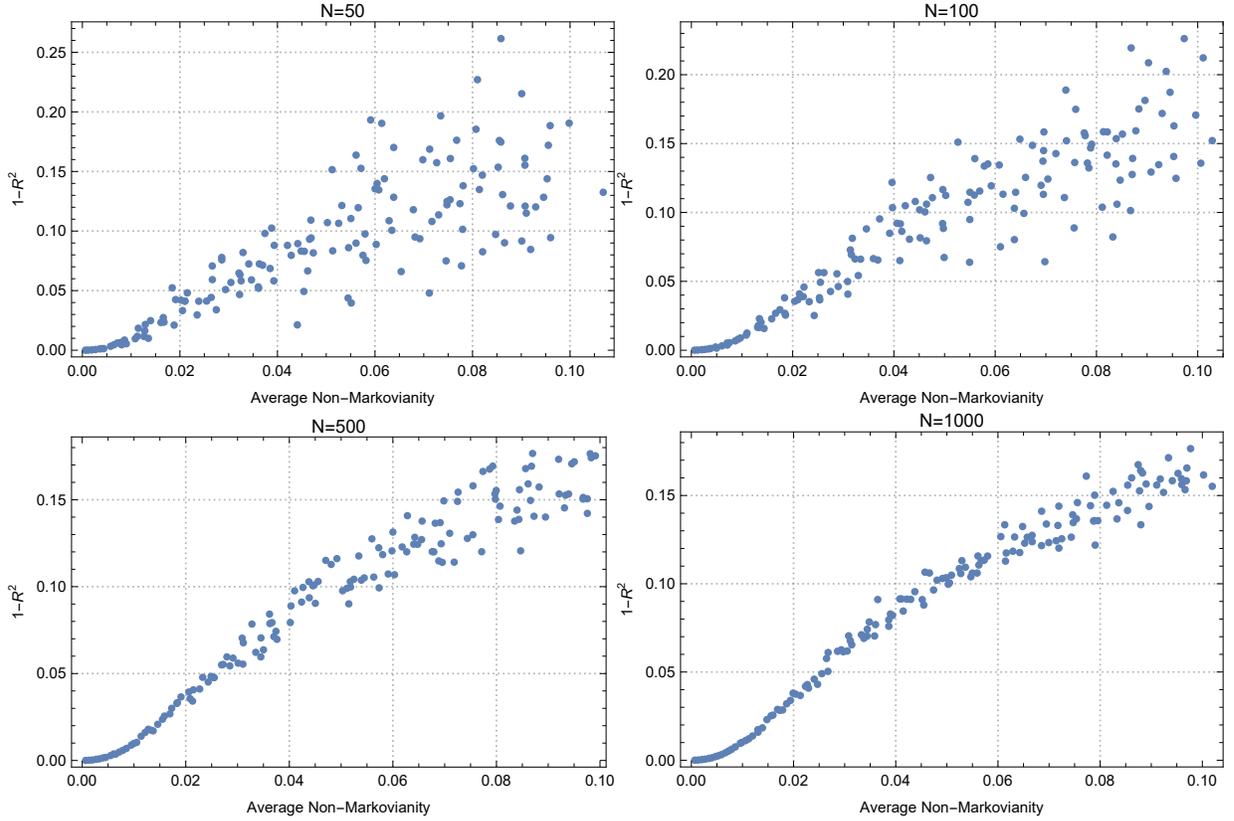
Figure 4.5: Comparison between the average non-Markovianity and the coefficient of determination of the exponential fit of the survival probability as a function of p_i's. In the simulation, p_i's are uniformly at random generated from the interval $[a, 1]$, as a decreases the average non-Markovianity decreases. Then $1 - R^2$ is plotted as a function of $\tilde{\xi}$, it can be seen from the plot when the number of p_i's (N) is big and the average non-Markovianity is small, $1 - R^2$ gives a relatively better estimate of $\tilde{\xi}$. Otherwise, the fluctuation of $1 - R^2$ around the same value of $\tilde{\xi}$ is quite large. For our randomized benchmarking simulation, $N = 2^5 = 32$, that means R^2 fluctuates a lot and the fluctuation depends even more on the scale of $\tilde{\xi}$.

4.4 Implementing the Clifford group

In order to efficiently implement the randomized benchmarking protocol, we need to use gates from the Clifford group. There are 24 elements in the Clifford group of one qubit, it is important to implement every element from the Clifford group precisely. The X and Z
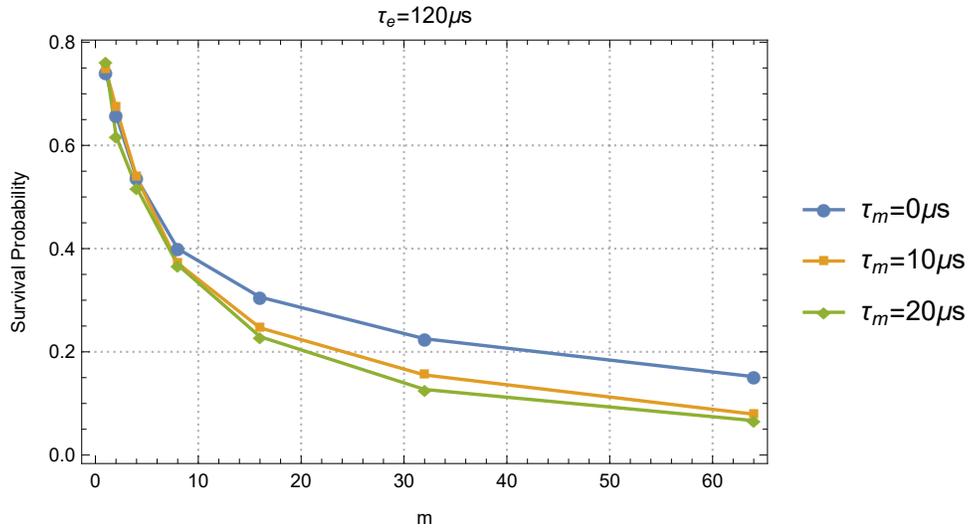
Figure 4.6: Some examples of survival probability of simulation of randomized benchmarking experiment with the same τ_e and different τ_m. It can be seen from the figure that when $\tau_m = 0\mu s$ the decay is more stretched, suggesting a large deviation from a single exponential decay. As τ_m increases, the non-Markovianity decreases and the decay becomes closer to a single exponential decay.
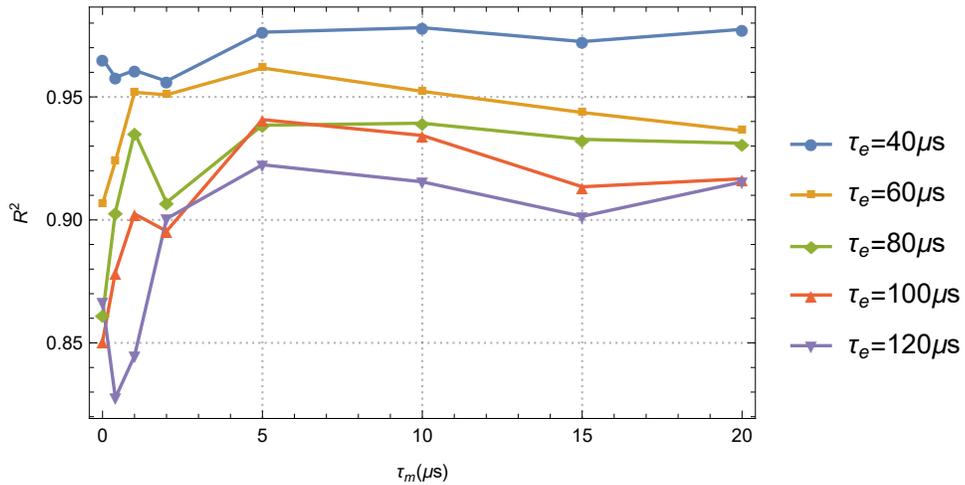
Figure 4.7: Coefficient of determination of single exponential fit of survival probability of randomized benchmarking simultaion with different configurations.

gates generate the whole Clifford group. And since Z gates can be efficiently implemented by changing the phase of the pulses, and for a well tuned spectrometer one can choose the phase of a pulse very precisely, we only need to optimize the X gate to achieve a precise implementation of the Clifford group [59]. On average, the X gate is implemented once for all Clifford gates, thus this approach does not increase the error. We need to minimize errors due to B_1 inhomogeneity and the heteronuclear interaction during the pulse. For B_1 inhomogeneity, we use the GRAPE algorithm [60] developed based on optimal control theory to find a shape pulse that is robust with respect to a range of Rabi frequency. The nonlinearity of the spectrometer is considered. Also the amplitude distortion is minimized by over-coupling the probe. The B_1 inhomogeneity measured with a Rabi experiment is about 24%, the fidelity of the shape pulse is optimized to cover the whole range of B_1 inhomogeneity. In Fig. 4.8, we compare the experimental results of flip-flip experiments implemented with a hard pulse and a robust shape pulse, it can be seen the decay due to B_1 inhomogeneity is greatly suppressed with the robust pulse. The heteronuclear interaction under the pulse gives every Clifford gate a non-Markovian gate-dependent error, but it can be decomposed into a sum of Markovian errors. In fact, when one implements a Clifford gate $C \otimes \mathbb{1}$ on the central spin, the Hamiltonian that generates the gate with noise can be written as
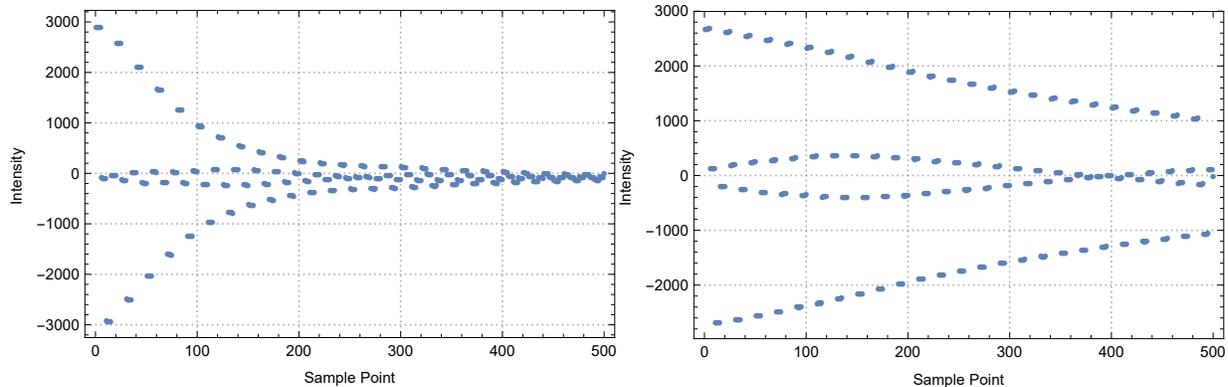
Figure 4.8: Proton signals obtained from flip-flip experiments with a hard pulse and a robust shape pulse. The experiments are implemented on water, the length of the hard pulse is $1.6\mu s$ while the length of the shape pulse is $9.6\mu s$. The outer lines of the data obtained with the shape pulse decay much slower than those of the hard pulse due to its robustness again B_1 inhomogeneity.

$$H = H_0(t) \otimes \mathbb{1} + V, \tag{4.59}$$

45

where

$$V = \sigma_z \otimes A, \tag{4.60}$$

with the condition that

$$\tilde{U}(t) = \mathcal{T}\left[e^{-i\int_0^t H_0(\tau)\otimes\mathbb{1}d\tau}\right],$$
$$\tilde{U}(t_0) = C \otimes \mathbb{1}. \tag{4.61}$$

Here, V generates the noise due to the heteronuclear interaction. Moving into the interaction frame defined by $\tilde{U}$, one obtains $H_I = \tilde{U}^\dagger V \tilde{U}$, according to the Lie product formula

$$U_I(t) = \mathcal{T}e^{-i\int_0^t H_I(\tau)d\tau} = e^{-i\int_0^t H_I(\tau)d\tau} + O(t^2). \tag{4.62}$$

Moving back to the ordinary frame we get

$$U(t) = \tilde{U}(t)U_I(t) = \tilde{U}(t)e^{-i\int_0^t H_I(\tau)d\tau} + O(t^2). \tag{4.63}$$

Therefore, if t_0 is relatively short, we have

$$U(t_0) \approx C \otimes \mathbb{1}e^{-i\int_0^{t_0} H_I(\tau)d\tau}, \tag{4.64}$$

and

$$\int_0^{t_0} H_I(\tau)d\tau = \delta_C \otimes A. \tag{4.65}$$

Therefore, using the local field picture, $U(t_0)$ is a CPTP map on each ρ_i. According to [61], Markovian gate dependent error has an exponentially weaker affect on the exponential decay. Therefore, except for the first few points, the gate dependent error does not has a prominent effect. Alternatively, we can design a shape pulse that simultaneously decouples σ_z under the pulse to the first order using the OCT algorithm with average Hamiltonian theory [62]. Note that under such a pulse the heteronuclear interaction is decoupled, and the pulse is automatically robust to other B_0 inhomogeneity.

46

Chapter 5

Conclusion and Future Work

5.1 Conclusion

In this thesis, some solid state NMR techniques have been introduced and used to study the change of local field in the central spin system. Due to the heteronuclear interaction between the central spin and the environment, the information is shared between them. By detecting the change of local field, we learned that information shared between the central spin and the environment is destroyed monotonically by the mixing caused by homonuclear interaction in the environment, which allows us to use a conditional probability to interpret the perturbation in the environment. After about $100\mu s$ of the mixing, the decay saturates. This is due to the symmetry of the mixing. In chapter four, we started by giving a general description of non-Markovian processes and a measure of the non-Markovianity ξ_d for ensemble systems and then generalize the method to the central spin system by taking the local field picture.

In order to quantify the non-Markovianity in the central spin system, we gave a measure based on measuring linearity of the process. Such a measure is metric-dependent and positive definite. A theory describing the effect of diffusion on the non-Markovianity was given, in which we proved that the diffusion destroys memory monotonically, resulting in less non-Markovianity. We generalized the theory to the central spin system and showed how the non-Markovianity would change given different correlation time and mixing time. We also showed that the average non-Markovianity, which is closely related to deviation from a single exponential decay of survival probability, gives a lower bound for the non-Markovianity. And we showed that by measuring the deviation from the single exponential

function, one can obtain a faithful estimation of the average non-Markovianity $\tilde{\xi}$ of the process when the system is large enough.

5.2 Future Work

We are still working on many subjects related to the material in this thesis.

First, average Hamiltonian theory is an old topic. However, the close relationship between control and decoupling suggests its application in quantum control theory. For instance, the theorem proved in chapter two can also be used in a quantum control theory: Given anti-Hermitians A, B and C, $\mathbb{1}B \in \text{span}_{\text{Lie}}\{A\mathbb{1} + \mathbb{1}B, C\mathbb{1}\}$, if and only if $\lim_{n\to\infty} e^{naA+Ct} = 0$ for some a and any t. On the other hand, quantum control can also be used in designing decoupling sequence, since all reachable average Hamiltonians are elements of the dynamical Lie algebra of the system. An interesting work is to connect this two areas explicitly.

For the third chapter, we want to obtain a 2D spectrum illustrating the change of local field. When there is no change of local field, the peaks should only appear along the line $\omega_1 = \omega_2$ (diagonal line) in the 2D spectrum. When there is mixing (change of local field), one should see off-diagonal peaks. Also, it is sufficient to project data onto the line $\omega_1 = -\omega_2$ to show the change of local field.

For the fourth chapter, we will do a randomized benchmarking experiment on the central spin system to test the theory. It is also interesting to explore in what cases the randomized benchmarking protocol gives a faithful estimation of the non-Markovianity.

References

[1] F. Petruccione and H. P. Breuer. *The theory of open quantum systems.* Oxford Univ. Press, 2002.

[2] W. F. Stinespring. Positive functions on C*-algebras. *Proc. Amer. Math. Soc.*, 6:211-216, 1955.

[3] M. A. Naimark. About second-kind self-adjoint extensions of symmetrical operator. *Izv. Akad. Nauk. SSSR Ser. Mat.*, 4:277-318, 1940.

[4] A. G. Redfield. On the theory of relaxation processes. *IBM J. Res. Dev.*, 1:19-31, 1957.

[5] A. G. Redfield. The theory of relaxation processes. *Adv. Magn. Reson.*, 1:1-32, 1965.

[6] S. Nakajima. On quantum theory of transport phenomena: steady diffusion. *Prog. Theo. Phys.*, 20: 948?59, 1958.

[7] R. Zwanzig. Ensemble method in the theory of irreversibility. *J. Chem. Phys.*, 33: 1338-1341, 1960.

[8] V. Gorini, K. Kossakowski, and E. Sudarshan. Completely positive dynamical semigroups of N-level systems. *J. Math. Phys. (N.Y.)*, 17:821, 1976.

[9] G. Lindblad. On the generators of quantum dynamical semigroups. *Commun. Math. Phys.*, 48:119-130 ,1976.

[10] P. W. Anderson. Spectral diffusion, phonons, and paramagnetic spin-lattice relaxation. *Phys. Rev.*, 114:10021005, 1959.

[11] J. R. Klauder and P. W. Anderson. Spectral diffusion decay in spin resonance experiments. *Phys. Rev.*, 125:912932, 1962.

[12] B. Herzog and E. L. Hahn. Transient nuclear induction and double nuclear resonance in solids. *Phys. Rev.*, 103:148166, 1956.

[13] S. K. Saikin, Wang Yao, and L. J. Sham. Single-electron spin decoherence by nuclear spin bath: Linked-cluster expansion approach. *Phys. Rev. B*, 75:125314, 2007.

[14] W. L. Ma, G. Wolfowicz, N. Zhao, S. S. Li, J. J. L. Morton, and R. B. Liu. Uncovering many-body correlations in nanoscale nuclear spin baths by central spin decoherence. *Nature Comm.*, 5:4822, 2014.

[15] W. Yao, R. Liu and L. J. Sham. Restoring coherence lost to a slow interacting mesoscopic spin bath. *Phys. Rev. Lett.*, 98:077602, 2007.

[16] W. Yang and R. Liu. Quantum many-body theory of qubit decoherence in a finite-size spin bath. *Phys. Rev. B*, 78:085315, 2008.

[17] W. Yang and R. Liu. Quantum many-body theory of qubit decoherence in a finite-size spin bath. II. Ensemble dynamics. *Phys. Rev. B*, 79:115320, 2009.

[18] M. Niknam. Dynamics of quantum information of the central spin problem. PhD diss., University of Waterloo, 2018.

[19] M. Niknam, L. F. Santos, and D. G. Cory. Sensitivity of quantum information to environment perturbations measured with the out-of-time-order correlation function. *arXiv:1808.04375v1*, 2018.

[20] S. R. Hartmann and E. L. Hahn. Nuclear double resonance in the rotating frame. *Phys. Rev.*, 128:2042-2053, 1962.

[21] W. K. Rhim, A. Pines, and J. S. Waugh. Time-reversal experiments in dipolar-coupled spin systems. *Phys. Rev. B*, 3:684-696, 1971.

[22] J. S. Waugh. Uncoupling of local field spectra in nuclear magnetic resonance: determination of atomic positions in solids. Proceedings of the National Academy of Sciences, 73(5):1394-1397, 1976.

[23] P. Caravatti, L. Braunschweiler, and R. R. Ernst. Heteronuclear correlation spectroscopy in rotating solids. *Chem. Phys. Lett.*, 100:305-310, 1983.

[24] U. Haeberlen. *High resolution NMR in solids selective averaging: supplement 1 advances in magnetic resonance. Vol. 1. Elsevier*, 2012.

[25] J. S. Waugh, L. M. Huber, and U. Haeberlen. Approach to high-resolution NMR in solids. *Phys. Rev. Lett.*, 20:180, 1968.

[26] U. Haeberlen and J. S. Waugh. Coherent averaging effects in magnetic resonance. *Phys. Rev.*, 175:453, 1968.

[27] P. Mansfield. Symmetrized pulse sequences in high resolution NMR in solids. *J. Phys. C*, 4:1444, 1971.

[28] W.K. Rhim, D. D. Elleman, and R. W. Vaughan. Analysis of multiple pulse NMR in solids. *J. Chem. Phys.*, 59:3740-3749, 1973.

[29] D. Burum and W. K. Rhim. Analysis of multiple pulse NMR in solids. III. *J. Chem. Phys.*, 71:944, 1979.

[30] D. G. Cory, J. B. Miller, and A. N. Garroway. Time-suspension multiple-pulse sequences: Applications to solid-state imaging. *J. Magn. Reson.*, 90:205-213, 1990.

[31] P. Mansfield and U. Haeberlen. Phase compensation in multi-pulse NMR experiments. *Z. Naturforsch. A*, 28:1081-1089, 1973.

[32] U. Haeberlen, J. D. Ellett Jr., And J. S. Waugh. Resonance offset effects in multiple-pulse NMR experiments. *J. Chem. Phys.*, 55:53, 1971.

[33] D.G. Cory , J.B. Miller , R. Turner, and A.N. Garroway. Multiple-pulse methods of ^{1}H NMR imaging of solids: Second-averaging. *Mol. Phys.*, 70:331-345, 1990.

[34] S. Idziak and U. Haeberlen. Design and construction of a high homogeneity rf coil for solid-state multiple-pulse NMR. *J. Magn. Reson.*, 50:281-288, 1982.

[35] B. C. Gerstein and C. R. Dybowski. *Transient techniques in NMR of solids: an introduction to theory and practice.* Academic Press, 1985.

[36] B. C. Gerstein. High-resolution NMR in solids with strong homonuclear dipolar broadening: Combined multiple-pulse decoupling and magic angle spinning. *Philos. Trans. R. Soc. London*, A299:521, 1981.

[37] W. K. Rhim, D. D. Elleman, L. Schreiber, and R. W. Vaughan. Analysis of multiple pulse NMR in solids. II. *J. Chem. Phys.*, 60:4595, 1974.

[38] D. P. Burum. M. Linder, and R. R. Ernst. Low-power multipulse line narrowing in solid-state NMR. *J. Magn. Reson.*, 43:173-188, 1981.

[39] P. Sun, J. Seland, and D. Cory. Background gradient suppression in pulsed gradient stimulated echo measurements. *J. Mag. Reson.*, 161:168-173, 2003.

[40] J. Tanner. Use of the stimulated echo in NMR diffusion studies. *J. Chem. Phys.*, 52:2523, 1970.

[41] H. Cho, P. Cappellaro, D. Cory, and C. Ramanathan. Decay of highly correlated spin states in a dipolar-coupled solid: NMR study of CaF_2. *Phys. Rev. B*, 74:224434, 2006.

[42] H. Cho, T. Ladd, J. Baugh, D. Cory, and C. Ramanathan. Multispin dynamics of the solid-state NMR free induction decay. *Phys. Rev. B*, 72:054427, 2005.

[43] W. Zhang and D. Cory. First direct measurement of the spin diffusion rate in a homogenous solid. *Phys. Rev. Lett.*, 80:1324, 1998.

[44] C. Ramanathan. Dynamic nuclear polarization and spin diffusion in nonconducting solids. *Appl. Magn. Reson.*, 34:409, 2008.

[45] G. Boutis, D Greenbaum, H. Cho, D. Cory, and C. Ramanathan. Spin diffusion of correlated two-spin states in a dielectric crystal. *Phys. Rev. Lett.*, 92:137201, 2004.

[46] A. Sodickson and D. Cory. A generalized k-space formalism for treating the spatial aspects of NMR experiments. *Prog. Nucl. Magn. Reson. Spectrosc.*, 33:77, 1998.

[47] P. G. Hoel, S. C. Port, and C. J. Stone. *Introduction to stochastic processes.*, Waveland Press, 1986.

[48] J. Emerson, R. Alicki, and K. Zyczkowski. Scalable noise estimation with random unitary operators. *J. Opt. B*, 7:S347, 2005.

[49] D. Gross, K. Audenaert, and J. Eisert. Evenly distributed unitaries: On the structure of unitary designs. *J. Math. Phs.*, 48:052194, 2007.

[50] C. Dankert, R. Cleve, J. Emerson, and E. Livine. Exact and approximate unitary 2-designs and their application to fidelity estimation. *Phys. Rev. A*, 80:012304, 2009.

[51] E. Magesan, J. Gambetta, and J. Emerson. Scalable and robust randomized benchmarking of quantum processes. *Phys. Rev. Lett.*, 106:180504, 2011.

[52] E. Magesan, J. Gambetta, and J. Emerson. Characterizing quantum gates via randomized benchmarking. *Phys. Rev. A*, 85:042311, 2012.

[53] W. K. Wootters and B. D. Fields. Optimal state-determination by mutually unbiased measurements. *Ann. Phys.*, 191:363, 1989.

[54] J. Emerson, M. Silva, O. Moussa, C. Ryan, M. Laforest, J. Baugh, D. Cory, and R. Laflamme. Symmetrized characterization of noisy quantum processes. Science 317:1893-1896, 2007.

[55] E. Magesan *et al.* Efficient measurement of quantum gate error by interleaved randomized benchmarking. *Phys. Rev. Lett.*, 109:080505, 2012.

[56] A. Abragam. *The principles of nuclear magnetism.* Oxford University Press, Oxford, 1961.

[57] A. Abragam, M. Goldman. *Nuclear magnetism: Order and disorder.* Clarendon Press, Oxford, 1982.

[58] D. Greenbaum. Magnetization and spin-spin energy diffusion in the XY model: A diagrammatic approach. *J. Magn. Reson.*, 179:11-19, 2006.

[59] D. McKay, C. Wood, S. Sheldon, J. Chow, and J. Gambetta. Efficient Z-Gates for quantum computing. *arXiv:1612.00858v2*, 2017.

[60] N. Khaneja, T. Reiss, C. Kehlet, T. Schulte-Herbrüggen, and S. Glaser. Optimal control of coupled spin dynamics: design of NMR pulse sequences by gradient ascent algorithms. *J. Magn. Reson.*, 172:296-305, 2005.

[61] J. Wallman. Randomized benchmarking with gate-dependent noise. *arXiv:1703.09835v2*, 2017.

[62] W. Rose, H. Haas, A. Chen, N. Jeon, L. Lauhon, D. Cory, and R. Budakian. High-Resolution nanoscale solid-State nuclear magnetic resonance spectroscopy. *Phys. Rev. X*, 8:011030, 2018.